

# Manganese dioxide nanosheets: from preparation to biomedical applications

This article was published in the following Dove Press journal:  
*International Journal of Nanomedicine*

Muyu Wu<sup>1,2,\*</sup>  
Pingfu Hou<sup>3,\*</sup>  
Lina Dong<sup>1</sup>  
Lulu Cai<sup>1</sup>  
Zhudian Chen<sup>1</sup>  
Mingming Zhao<sup>1</sup>  
Jingjing Li<sup>1,2,4</sup>

<sup>1</sup>School of Medical Imaging, Xuzhou Medical University, Xuzhou 221004, Jiangsu, People's Republic of China; <sup>2</sup>Department of Radiology, Affiliated Hospital of Xuzhou Medical University, Xuzhou 221006, Jiangsu, People's Republic of China; <sup>3</sup>Jiangsu Center for the Collaboration and Innovation of Cancer Biotherapy, Cancer Institute, Xuzhou Medical University, Xuzhou 221004, Jiangsu, People's Republic of China; <sup>4</sup>Institute of Medical Imaging and Digital Medicine, Xuzhou Medical University, Xuzhou 221004, Jiangsu, People's Republic of China

\*These authors contributed equally to this work

**Abstract:** Advancements in nanotechnology and molecular biology have promoted the development of a diverse range of models to intervene in various disorders (from diagnosis to treatment and even theranostics). Manganese dioxide nanosheets (MnO<sub>2</sub> NSs), a typical two-dimensional (2D) transition metal oxide of nanomaterial that possesses unique structure and distinct properties have been employed in multiple disciplines in recent decades, especially in the field of biomedicine, including biocatalysis, fluorescence sensing, magnetic resonance imaging and cargo-loading functionality. A brief overview of the different synthetic methodologies for MnO<sub>2</sub> NSs and their state-of-the-art biomedical applications is presented below, as well as the challenges and future perspectives of MnO<sub>2</sub> NSs.

**Keywords:** MnO<sub>2</sub> nanosheets, synthetic methods, biocatalysis, fluorescence sensing, controlled drug delivery, stimuli-activated imaging

## Introduction

Advances in nanotechnology and molecular biochemistry, the ability to decrypt and elaborate multiple artificial materials, the continuous search for new targets, and the disentangling of diverse signaling pathways of many medical disorders have had a conspicuous influence on modern medical practices.<sup>1-4</sup> Among the various nanomaterials designed for biomedical applications, two-dimensional (2D) materials, especially transition metal dichalcogenides (eg, MoS<sub>2</sub>, WS<sub>2</sub>, TiS<sub>2</sub>, MoSe<sub>2</sub>, and WSe<sub>2</sub>)<sup>5</sup> and transition metal oxides (TMOs, eg, MnO<sub>2</sub>),<sup>6</sup> have received a substantial amount of recent attention due to their distinct structure–property relationships in multiple fields, eg, optoelectronics, spintronics, catalysis, defect engineering, and energy-related applications.<sup>7-9</sup> Among these materials, manganese oxides have attracted increasing attention because Mn is the twelfth most common element on the planet and the third most abundant transition element after iron and titanium.<sup>10</sup> Manganese (II) ions function as cofactors in a number of enzymes with varying functionalities as well as being key components in the oxygen-evolving complexes of photosynthetic plants.<sup>11</sup> Additionally, manganese oxide (Mn-oxide) has a variety of structures (nanorods, nanobelts, nanosheets (NSs), nanowires, nanotubes, nanofibers and so on)<sup>12</sup> and compositions (MnO, Mn<sub>5</sub>O<sub>8</sub>, Mn<sub>2</sub>O<sub>3</sub>, MnO<sub>2</sub>, and Mn<sub>3</sub>O<sub>4</sub>)<sup>13</sup> which further broadens its applications in a diverse range of fields. Hoseinpour et al reviewed the structures, sizes and applications of Mn NPs prepared via different green synthetic methods in detail.<sup>14</sup> Among the various nanostructures, NS is two-dimensional nanostructure with thickness ranging from 1 to 100 nm. A typical NS example is graphene, which is composed of a single layer of carbon atoms with hexagonal lattice.<sup>15</sup> NS shares several

Correspondence: Jingjing Li  
Department of Radiology, Affiliated Hospital of Xuzhou Medical University, 99 Huaihai West Road, Xuzhou 221006, People's Republic of China  
Tel +8651683262623  
Email qingchao0124@163.com

similar common features, eg, ultralarge specific surface areas and high surface-to-volume ratios, allowing easy contact between reactant molecules and the active sites, thus providing enhanced catalytic activities<sup>16</sup> as well as unique optical properties (described below) and excellent photothermal therapy (PTT), etc.<sup>17</sup> MnO<sub>2</sub> nanosheets (MnO<sub>2</sub> NSs) are composed of MnO<sub>6</sub> octahedra that share edges, with manganese ions occupying the centers of the octahedra and being coordinated to the six nearest oxygen ions, while each oxygen ion is coordinated to the three nearest manganese ions.<sup>18,19</sup> Similar to the structures of other 2D materials, MnO<sub>2</sub> NSs possess high specific surface areas and a thickness of nanometers to micrometers. Moreover, the redox reactions between MnO<sub>2</sub> and glutathione (GSH) in acidic environment have favored their applications in activatable fluorescent biosensors, controlled drug delivery and activatable T<sub>1</sub>-MR imaging.<sup>20–22</sup> As a class of novel and facilely synthesized 2D TMOs with good biocompatibility, MnO<sub>2</sub> NSs have received increased attention across a vast range of disciplines, especially biomedicine. In this review, we aim to provide an overview of the state-of-the-art syntheses, biomedical applications, toxicological assessments and challenges/opportunities in the research field of MnO<sub>2</sub> NSs. First, various synthetic strategies for the preparation of MnO<sub>2</sub> NSs are introduced. Then, we briefly discuss their main biomedical applications. Furthermore, the *in vitro* and *in vivo* toxicological evaluations are highlighted. Ultimately, we provide some personal perspectives on the future directions of this promising research field.

## Synthesis of manganese dioxide nanosheets (MnO<sub>2</sub> NSs)

As a class of 2D nanomaterials, NSs are characterized by their nanometer thicknesses as well as lateral dimensions ranging from the submicrometers to micrometer scales. MnO<sub>2</sub> NSs with extremely large surface-area-to-mass ratios (SMRs) display a number of distinctive physicochemical properties compared with their bulk form. Hence, the synthesis of MnO<sub>2</sub> NSs is of great significance for a variety of novel biomedical applications. To date, several methods have been developed for the preparation of MnO<sub>2</sub> NSs. In general, these methods can be classified into two categories: top-down and bottom-up approaches, as is also true of other types of 2D nanomaterials.<sup>23</sup> In 2003, Omomo et al. first reported the formation and characterization of unilamellar 2D crystallites of MnO<sub>2</sub> as well as the swelling and exfoliation behavior of layered

manganese oxide, H<sub>0.13</sub>MnO<sub>2</sub>·H<sub>2</sub>O, which was dissolved in tetrabutylammonium hydroxide solution.<sup>24</sup> This traditional top-down approach always utilizes ion-exchange and exfoliation of bulk MnO<sub>2</sub> templates to obtain MnO<sub>2</sub> NSs. However, this route entails a cost-demanding and time-consuming multistep high-temperature solid-state synthetic process. Moreover, one hurdle that the obtained NSs possess a wide thickness distribution, which is a challenge that must be overcome before their possible future application. In 2008, Kazuya Kai et al demonstrated a single-step bottom-up approach to directly synthesize MnO<sub>2</sub> NSs for the first time,<sup>25</sup> drawing from the synthetic methodology for producing Ti<sub>1-δ</sub>O<sub>2</sub> monosheets with uniform shapes and sizes reported by Yoon and coworkers.<sup>26</sup> Since then, the bottom-up strategy, as a novel approach to synthesize MnO<sub>2</sub> NSs, has attracted the attention of most researchers in this field, owing to its significant advantages, such as an easier preparation and better controlled exfoliation and reaction steps. In this review, we focus on the bottom-up methods for obtaining MnO<sub>2</sub> NSs, and their sizes and morphologies when prepared by different approaches have been summarized in Table 1.

## Manganese ion (Mn<sup>2+</sup>) based oxidative methodology

The preparation of multilayer MnO<sub>2</sub> NSs (ca. 10 nm in thickness) with bottom-up approaches has mainly been achieved by the oxidation of Mn<sup>2+</sup> or the reduction of KMnO<sub>4</sub> with a self-sacrificing template (eg, graphene oxide nanosheets; GO NSs) or a chelating agent (eg, EDTA)<sup>27</sup> in the presence of reducing or oxidizing reagents. In 2007, Oaki and Imai proposed bottom-up approach to obtain MnO<sub>2</sub> NSs by the oxidation of manganese ions with dissolved oxygen in the solution.<sup>27</sup> EDTA was utilized as a chelating agent for the manganese ions (Mn<sup>2+</sup>) to hinder the rapid precipitation of Mn(OH)<sub>2</sub>. However, their precipitate consisted of multiple layers with thicknesses of 10 nanometers or greater (ie, over 10 layers). Moreover, the time-consuming process (at least 3 days) was unavoidable. To address these issues, inspired by the single-step route reported by Yoon for the synthesis of titanate dioxide nanosheets (Ti<sub>1-δ</sub>O<sub>2</sub> NSs), Kazuya Kai and coworkers attempted to prepare MnO<sub>2</sub> NSs with hydrogen peroxide (H<sub>2</sub>O<sub>2</sub>) as an oxidant in an alkaline medium and TMA cations for the exfoliation of layered H/MnO<sub>2</sub>. However, unlike the method from Yoon, their reaction readily proceeded at ambient temperature instead of heating under reflux (Figure 1).<sup>26</sup>

Table 1 Summarized sizes and morphologies of MnO<sub>2</sub> NSs synthesized by different approaches

Method	Reaction materials	Morphology	Lateral dimensions	Thickness	Reference
Top-Down	H <sub>0.13</sub> MnO <sub>2</sub> ·0.7H <sub>2</sub> O + TBAOH	Nanosheet structure	<50 nm	0.91 ± 0.07 nm	24
Bottom-Up (reductive)	KMnO <sub>4</sub> + MES	Nanosheet structure	141 nm	~1.5 nm	28
Bottom-Up (reductive)	KMnO <sub>4</sub> + SDS	Single-layered nanosheet	~200 nm	0.77–0.95 nm	29
Bottom-Up (oxidative)	MnCl <sub>2</sub> + EDTA + NaOH	Thin film of nanosheet	2–5 μm width	~10 nm	27
Bottom-Up (oxidative)	MnCl <sub>2</sub> + TMAOH	Single-layered NS	<200 nm	Nearly 80% < 1 nm	25
Bottom-Up (oxidative)	MnCl <sub>2</sub> + H <sub>2</sub> O <sub>2</sub> + TMAOH	A two-dimensional sheet structure	~200 nm	~1.3 nm.	111
Bottom-Up (oxidative)	MnCl <sub>2</sub> + (NH <sub>4</sub> ) <sub>2</sub> S <sub>2</sub> O <sub>8</sub> + TMAOH	Flat morphology	2 μm	~4.07 nm	35
Bottom-Up (oxidative)	MnCl <sub>2</sub> + H <sub>2</sub> O <sub>2</sub> + TMAOH	A sheet-like structure	N/A	~1.5 nm	36
Bottom-Up (oxidative)	MnCl <sub>2</sub> + H <sub>2</sub> O <sub>2</sub> + TMAOH	Nanosheet structure	100–200 nm	N/A	69
Bottom-Up (oxidative)	MnCl <sub>2</sub> + H <sub>2</sub> O <sub>2</sub> + TMAOH	Polycrystalline sheet structure	141 nm	1.5 nm	150
Bottom-Up (oxidative)	MnCl <sub>2</sub> + H <sub>2</sub> O <sub>2</sub> + TMAOH	Single-layer sheet structure	200 nm	~1.5 nm	170

Abbreviations: TMAOH, tetramethylammonium hydroxide; TBAOH, tetrabutylammonium hydroxide; NS, nanosheet.

## Potassium permanganate (PP, KMnO<sub>4</sub>)-based reductive methodology

Compared to the top-down and the oxidative bottom-up methods, a reductive bottom-up method has been developed in recent years. With KMnO<sub>4</sub> as the Mn source, different reactive agents have been introduced to prepare MnO<sub>2</sub> NSs. For example, Liu et al first obtained MnO<sub>2</sub> NSs via the addition of an aqueous KMnO<sub>4</sub> solution into a 2-(N-morpholino)ethanesulfonic acid (MES) buffer at pH 6. Compared with other reducing reagents (eg, MnCl<sub>2</sub> and ethanol), the use of the MES buffer as the reducing agent showed the best results (Figure 2A).<sup>28</sup> Later, in 2015, Yin and coworkers developed a facile template-free, one-step and one-phase reductive strategy to synthesize single-layered MnO<sub>2</sub> NSs with sodium dodecylsulfate (SDS) as the reducing agent. In their system, SDS not only played the role of a precursor of dodecanol to reduce KMnO<sub>4</sub> but also was a structure-directing agent to promote the formation of the MnO<sub>2</sub> monosheets, which opened up the possibility of constructing other NS without the use of an exfoliation reagent (Figure 2B).<sup>29</sup> Indeed, this reductive method was more facile in both principle and practice because a variety of reductants could be selected. Furthermore, the synthetic process for the MnO<sub>2</sub> NSs was more controllable. Nonetheless, an inevitable drawback was that KMnO<sub>4</sub> tended to decompose in hydrothermal environments (*ca.* 95°C), which challenged researchers attempting to verify the exact mechanisms of the corresponding chemical reactions.<sup>30–34</sup>

## Biomedical applications of MnO<sub>2</sub> nanosheets (MnO<sub>2</sub> NSs)

Since the intriguing 2D structure and distinct physical/chemical properties were initially identified, MnO<sub>2</sub> NSs have received much attention and have exhibited favorable potential for application in a wide range of disciplines, such as physics,<sup>37</sup> chemistry,<sup>38</sup> material science<sup>39</sup> (especially energy-related applications, eg, solar cells,<sup>40</sup> supercapacitors,<sup>41–45</sup> and lithium-ion batteries<sup>46,47</sup>), optoelectronics,<sup>48,49</sup> spintronics,<sup>18</sup> biomedicine,<sup>40</sup> and so forth. Particularly, their broad use in biological sensing and catalysis, drug delivery and controlled release, PTT and chemo-dynamic therapy (CDT),<sup>21</sup> molecular imaging and engineering, etc., has shown promising potential. Herein, we summarize a majority of the MnO<sub>2</sub> NS applications in recent years in the field of biomedicine (Figure 3).

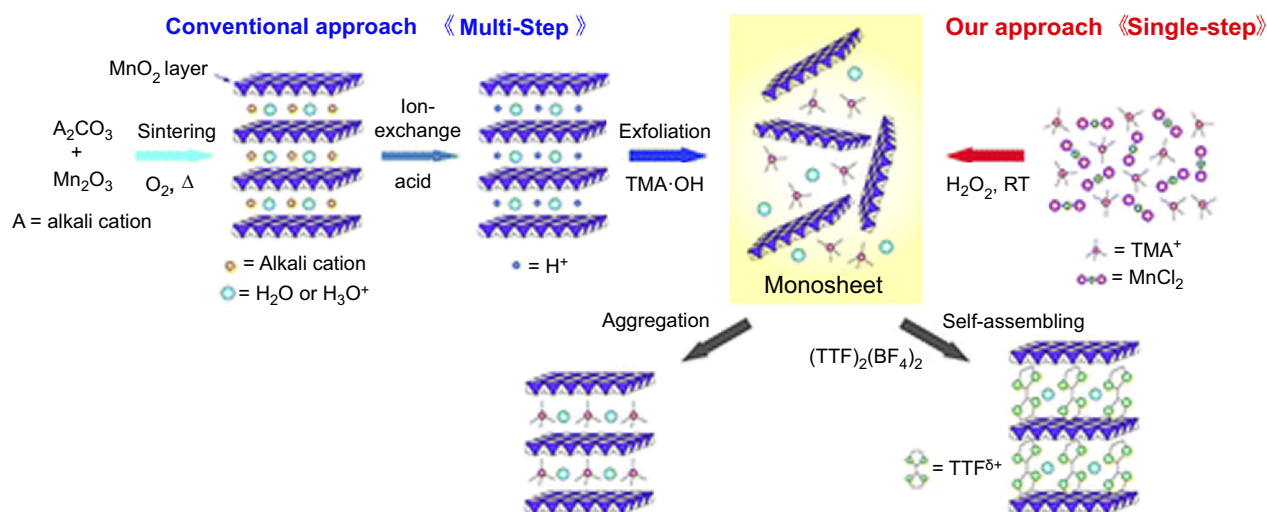


**Figure 1** Schematic illustration of the single-step oxidative method with  $\text{H}_2\text{O}_2$  at room temperature versus the conventional method.

**Note:** Reprinted with permission from Kai K, Yoshida Y, Kageyama H, et al. Room-temperature synthesis of manganese oxide monosheets. *J Am Chem Soc.* 2008;130(47):15938–15943.<sup>25</sup> Copyright (2008) American Chemical Society.

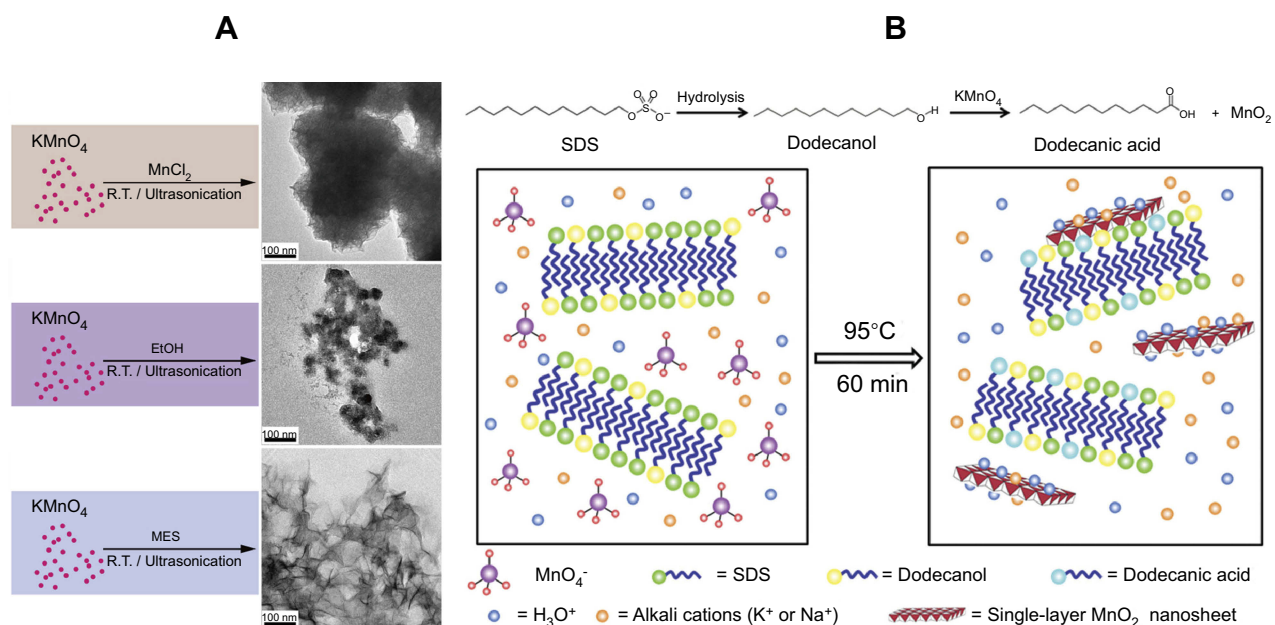


**Figure 2 (A)** Schematic illustration for the control experiments of reductants employed in the growth of  $\text{MnO}_2$  nanomaterials at ambient temperature (left) and TEM characterization of the corresponding products (right). Reprinted with permission from Deng R, Xie X, Vendrell M, Chang Y, Liu X. Intracellular glutathione detection using  $\text{MnO}_2$ -nanosheet-modified upconversion nanoparticles. *J Am Chem Soc.* 2011;133(50):20168–20171.<sup>28</sup> Copyright 2011 American Chemical Society. **(B)** Schematic illustration for  $\text{MnO}_2$  NS formation based on the  $\text{KMnO}_4$  and SDS reaction. Reprinted with permission from Liu Z, Xu K, Sun H, Yin S. One-step synthesis of single-layer  $\text{MnO}_2$  nanosheets with multi-role sodium dodecyl sulfate for high-performance pseudocapacitors. *Small.* 2015;11(18):2182–2191.<sup>29</sup> Copyright © 2015, John Wiley and Sons.

## As a nanozyme: biocatalysis based on $\text{MnO}_2$ NSs

In recent decades, nanotechnology and biochemistry have flourished, including artificial materials with multiple applications.<sup>7,50,51</sup> Certain nanomaterials possess enzymatic-like profiles and substrate specificities, which are commonly called “Nanozymes”. Despite the substrate specificities of nanozymes rarely being as high as those of natural enzymes,

their multiple active sites favor more efficient and steady catalytic activity. Additionally, owing to their tunable structures, their related properties can be controlled and optimized.<sup>52,53</sup> Furthermore, compared with natural enzymes, nanozymes are more compatible with specific environments, such as high temperatures, and low or high pH conditions.<sup>54</sup> These features give rise to their promising applications in a variety of fields.

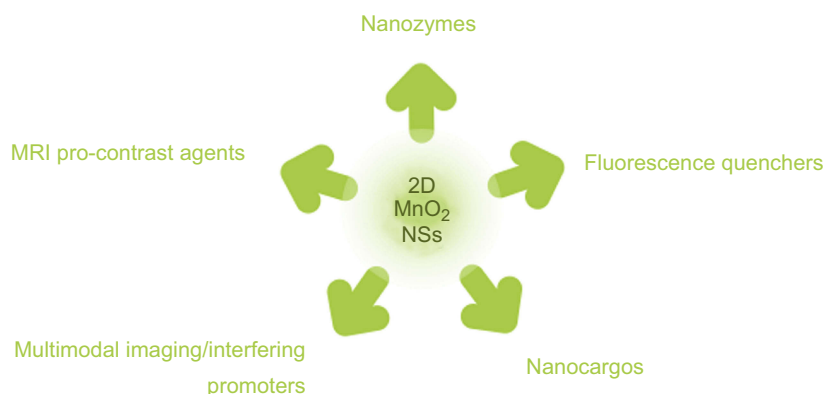


**Figure 3** Schematic illustration of the diverse roles  $\text{MnO}_2$  NSs have played in the field of biomedicine.

Nanozymes, mainly comprising carbon,<sup>55,56</sup> metal,<sup>57,58</sup> and metal oxide,<sup>59,60</sup> mimic the functionality of natural enzymes, but have different structures. Amongst them, 2D nanomaterials,<sup>61</sup> with ultralarge surface areas and flexible structures, enable their excellent catalytic activity and can be incorporated into the surrounding environment to improve substrate specificity. For instance, graphene oxide has been confirmed to possess intrinsic peroxidase-like activity in the presence of hydrogen peroxide ( $\text{H}_2\text{O}_2$ ),<sup>62,63</sup> so as to ultrathin graphitic carbon nitride (g-CN)<sup>64,65</sup> and molybdenum disulfate nanosheets ( $\text{MoS}_2$  NSs),<sup>66</sup> which are only pragmatic for use as *ex-vivo* or *in vitro* substrates.  $\text{MnO}_2$  NSs, a typical 2D nanomaterial, also possess intrinsic oxidase-like activity. In 2012, Liu and Wang et al. employed 3,3',5,5'-tetramethylbenzidine (TMB) as a tracer to test this property.<sup>67</sup> The oxidation of the pale yellow-

colored substrate (TMB) to the blue-oxidized product (ox-TMB) indicated the catalytic activity of the  $\text{MnO}_2$  NSs. Based on this, Liu and colleagues have developed a selective, rapid, and reliable colorimetric assay for the determination of GSH because GSH can further lead to a concentration-dependent reduction of ox-TMB and a proportional decrease in the absorption at ca. 650 nm (Figure 4A).<sup>68</sup> Notwithstanding their utilization as a group of nanozymes with oxidase activity,  $\text{MnO}_2$  NSs can also act as indirect DNA partzymes to some extent. Recently, Zhao et al fabricated a  $\text{MnO}_2$  NS-powered target/probe Janus protected DNA nanomachine to achieve RNA imaging. In this DNA machine, the  $\text{MnO}_2$  NSs were utilized as both promoters for the cellular uptake of DNA and generators of  $\text{Mn}^{2+}$  as indispensable DNAzyme cofactors, ensuring the efficiency of catalytic cleavage (Figure 4B).<sup>69</sup>

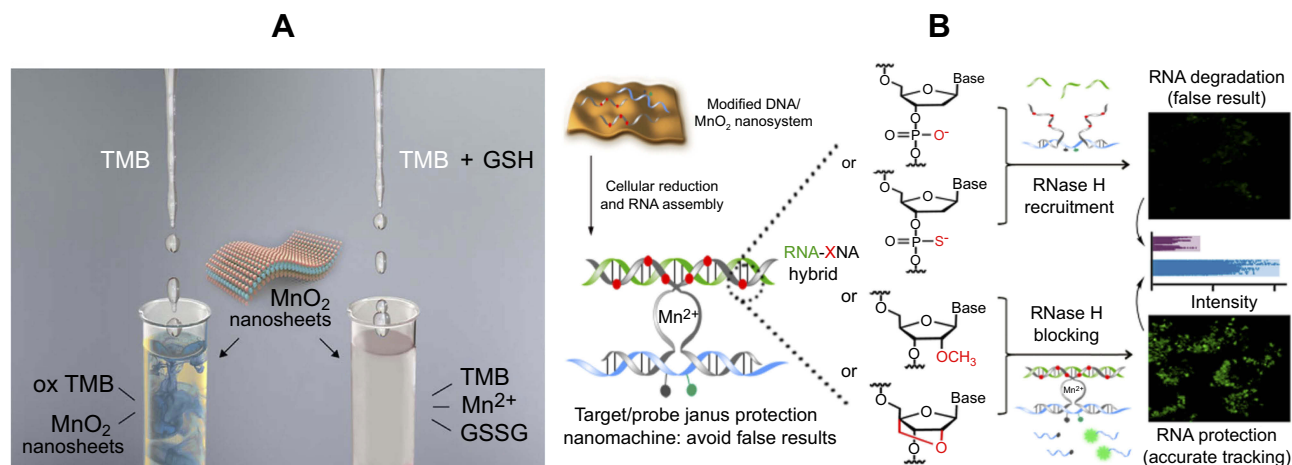


**Figure 4** (A) Illustration of the  $\text{MnO}_2$  NS-based colorimetric assay for GSH quantification, where the  $\text{MnO}_2$  NSs acted as an oxidase-like nanozyme for the formation of ox-TMB and GSSG. Reprinted from *Biosensors and Bioelectronics*, 90, Liu J, Meng L, Fei Z, Dyson P, Jing X, Liu X.  $\text{MnO}$  nanosheets as an artificial enzyme to mimic oxidase for rapid and sensitive detection of glutathione, 69–74, Copyright (2017), with permission from Elsevier.<sup>68</sup> (B) Schematic design of the Janus protected DNA nanomachine, where miRNA-21 is employed as a model cellular RNA target (green sequence), the red X denotes DNA, PS (phosphorothioate)-DNA, 2'OMe (methylation)-DNA and LNA (locked nucleic acid) monomers, which are highlighted in the DNA partzymes (gray sequences). Reprinted with permission from Chen F, Bai M, Zhao Y, Cao K, Cao X, Zhao Y.  $\text{MnO}$ -nanosheet-powered protective janus DNA nanomachines supporting robust RNA imaging. *Anal Chem*. 2018;90(3):2271–2276.<sup>69</sup> Copyright 2018 American Chemical Society.

## As a quencher: fluorescence sensing based on MnO<sub>2</sub> NSs

The use of 2D nanomaterials with light harvesting and/or electron-conducting capacities has emerged as a promising nanoplatform for biological and/or chemical sensing based on the fluorescence resonance energy transfer (FRET), photoinduced transfer mechanisms, etc.<sup>70,71</sup> Fluorescence or Förster resonance energy transfer (FRET) is a mechanism delineating nonradiative energy transfer<sup>72</sup> from a luminescent donor to an energy acceptor in proximity (ie, 1–10 nm) mediated by dipole-dipole coupling.<sup>73,74</sup> Due to its high sensitivity and suitability for homogeneous detection, FRET has been universally utilized in a variety of fields, eg, microscope,<sup>75</sup> immunoassay,<sup>76,77</sup> nucleic acid hybridization<sup>78–81</sup> and macromolecule interactions.<sup>82,83</sup> As a 2D nanomaterial as well as an ultrathin semiconductor, MnO<sub>2</sub> NSs exhibit a broad and intense absorption band at ca. 374 nm,<sup>24</sup> making them as an efficient broad-spectrum quencher, which is resulted from the d–d transitions of manganese ions in the ligand field of the edge-sharing MnO<sub>6</sub> octahedral crystal lattice.<sup>24</sup> The use of MnO<sub>2</sub> NSs as fluorescence quencher can mainly be ascribed to two aspects: their broad and intense absorption band at ca. 374 nm and the break-up of the NSs structure with the reduction of MnO<sub>2</sub> into Mn<sup>2+</sup>. Ji et al designed a multifunctional nanosystem, CaO<sub>2</sub>/MnO<sub>2</sub>@polydopamine-methylene blue (MB) nanosheets (CMP-MB), where the fluorescence of MB was suppressed by the MnO<sub>2</sub> NS. Once exposed to a tumor microenvironment, the MnO<sub>2</sub> NSs could decompose into Mn<sup>2+</sup>, which triggered the emission of MB fluorescence. Hence, switch-controlled tumor cell imaging was achieved.<sup>84</sup> Xia et al. found that the MnO<sub>2</sub> NS mediated quenching effect can be reversed via the reduction of MnO<sub>2</sub> into Mn<sup>2+</sup> by ascorbic acid (AA), resulting in MnO<sub>2</sub> NS destruction. Based on this, they developed a carbon dot (CD)-MnO<sub>2</sub> nanocomposite for the determination of ALP with help from the hydrolysis of 2-phosphate (AAP) into AA. Utilizing the CD-MnO<sub>2</sub> nanocomposite as a sensing probe, a label-free fluorescent switching strategy for detecting ALP activity was realized with a limit of detection (LOD) of 0.4 U/L.<sup>85</sup> In 2015, with the reduction of MnO<sub>2</sub> into Mn<sup>2+</sup> by GSH, Wang and coworkers employed fluorescent CDs and MnO<sub>2</sub> NSs as an energy donor-acceptor pair to construct a nanoplatform for GSH detection (Figure 5A).<sup>86</sup> In addition to employing MB and CDs as fluorescence donors, Yan et al fabricated a graphene quantum dot (GQD)-MnO<sub>2</sub> NS-based optical sensing platform for GSH detection (Figure 5B).<sup>87</sup>

Chu and colleagues developed a MnO<sub>2</sub> NS-modified upconversion (UC) nanosystem for sensitive switchable fluorescence detection of H<sub>2</sub>O<sub>2</sub> and glucose in blood. The enzymatic cleavage and unification of glucose by glucose oxidase (GOx) generated H<sub>2</sub>O<sub>2</sub>, which was then utilized to reduce MnO<sub>2</sub> to Mn<sup>2+</sup>, similarly to GSH (as depicted by the equation: MnO<sub>2</sub> + H<sub>2</sub>O<sub>2</sub> + 2H<sup>+</sup> = Mn<sup>2+</sup> + 2H<sub>2</sub>O + O<sub>2</sub>) (Figure 5C).<sup>88</sup>

In addition to sensing relatively more tractable and visible substances, such as GSH and H<sub>2</sub>O<sub>2</sub>, MnO<sub>2</sub> NSs can also be utilized for tracking RNAs even at very low levels. As is well-known, miRNAs can regulate gene expression by promoting the degradation or inhibition of the translation of target messenger RNAs (mRNAs) in epigenetics,<sup>89–91</sup> thereby playing momentous roles in cell differentiation,<sup>92–95</sup> proliferation,<sup>96</sup> tumorigenesis,<sup>97,98</sup> metastasis,<sup>99,100</sup> apoptosis,<sup>98</sup> autophagy<sup>101,102</sup> and many other biochemical processes. Despite quantitative determination of various miRNAs being accomplished by traditional detection strategies, eg, PCR and northern blot, these previously developed methods possess unavoidable costs and are time-consuming as well as having sensitivity limiting shortcomings. Therefore, recent alternatives have incorporated a variety of signal amplification approaches such as nanomaterials,<sup>80,103–106</sup> enzymes,<sup>107</sup> electrochemical<sup>108</sup> or electrochemiluminescent<sup>109</sup> transduction fashion to detect target miRNAs with both high selectivity and high sensitivity. In 2017, Xiang and colleagues reported a biodegradable MnO<sub>2</sub> NS-based hybridization chain reaction (HCR) strategy to determine miRNA expression even at exceedingly low levels in living cells.<sup>110</sup> They designed two hairpins which were separately labeled with the organic dyes FAM (as a FRET donor) and Tamra (TMR, as a FRET acceptor) and loaded onto MnO<sub>2</sub> NSs. Thereafter, once entering living cells, the hairpins would be released because of the displacement responses as well as the degradation of the MnO<sub>2</sub> NSs by intracellular GSH. Then, miRNA-21 in living HeLa cells triggered the hairpins to convene into double-stranded polymers, resulting in prominent amplification of the FRET signal for the determination of trace levels of miRNA-21 in living cells (Figure 6).<sup>111</sup> It is anticipated that this inspiring work might open up new opportunities for monitoring multiple trace-level RNA species in living cells with greater accuracy, sensitivity and integrity.

Finally, the applications of various MnO<sub>2</sub> NS-based fluorescent biosensors for determining specific targets are

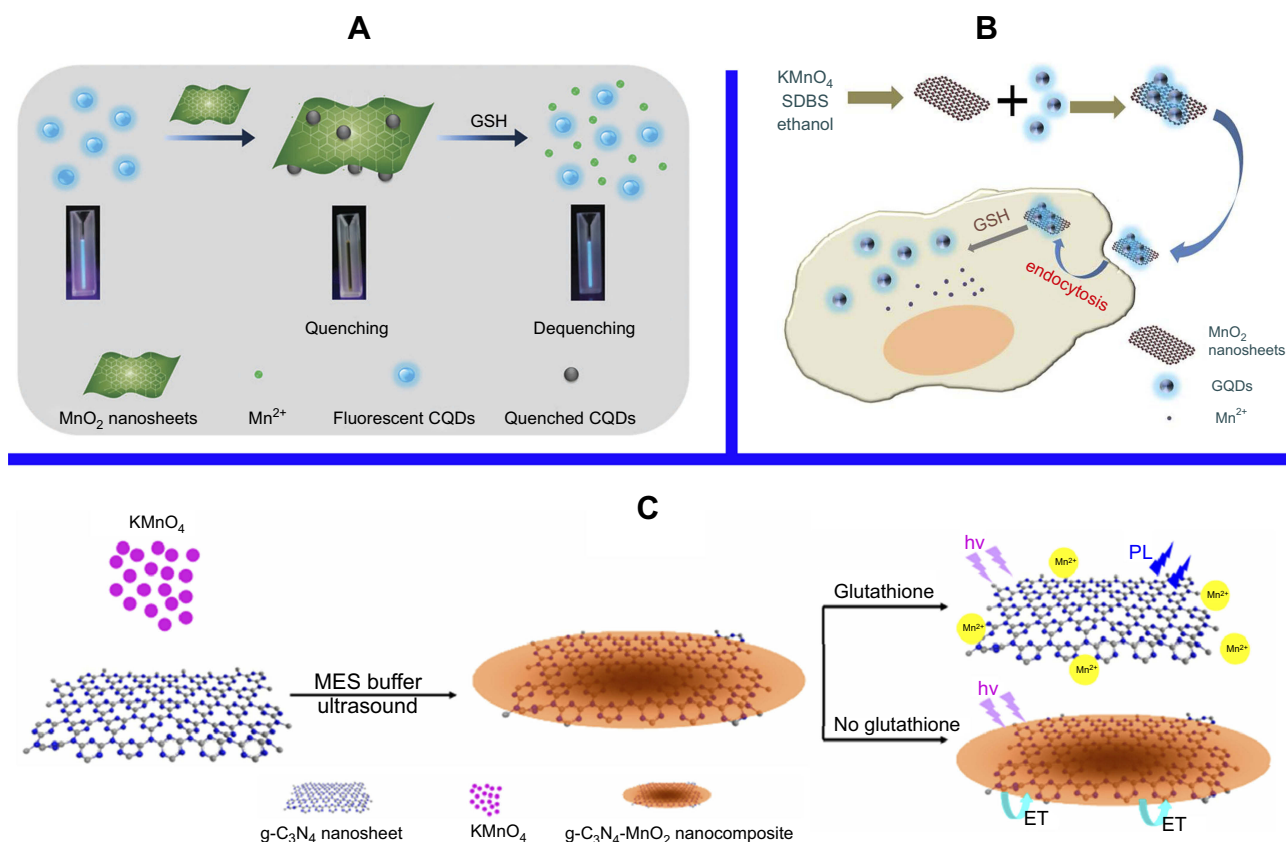


**Figure 5** (A) Schematic illustration of the preparation of CDs-MnO<sub>2</sub> NSs and the principle of the FRET-based CD-MnO<sub>2</sub> NSs architecture for GSH sensing. Republished with permission of Royal Society of Chemistry, from A sensitive turn-on fluorescent probe for intracellular imaging of glutathione using single-layer MnO<sub>2</sub> nanosheet-quenched fluorescent carbon quantum dots, He D, Yang X, He X, et al, 51, 79, 2015; permission conveyed through Copyright Clearance Centre, Inc.<sup>170</sup> (B) Scheme for the preparation of MnO<sub>2</sub> NSs and the mechanism of a GQD-MnO<sub>2</sub> NS-based optical sensing nanoplatfor for monitoring GSH in MCF-7 cells. Reprinted with permission from Yan X, Song Y, Zhu C, et al. Graphene quantum dot-MnO<sub>2</sub> nanosheet based optical sensing platform: a sensitive fluorescence “Turn Off-On” nanosensor for glutathione detection and intracellular imaging. *ACS Appl Mater Interfaces*. 2016;8(34):21990–21996.<sup>87</sup> Copyright 2016 American Chemical Society. (C) Schematic illustration of a g-C<sub>3</sub>N<sub>4</sub> NS-MnO<sub>2</sub> NS sandwich-like nanocomposite for GSH sensing. Reprinted with permission from Zhang X, Zheng C, Guo S, Li J, Yang H, Chen G. Turn-on fluorescence sensor for intracellular imaging of glutathione using g-C<sub>3</sub>N<sub>4</sub> nanosheet-MnO<sub>2</sub> sandwich nanocomposite. *Anal Chem*. 2014;86(7):3426–3434.<sup>151</sup> Copyright 2014 American Chemical Society.

listed in Table 2, and their different values for the limits of detection (LODs) as well as the linear concentration ranges of the corresponding targets are mentioned.

### As a nanocarrier for controlled drug delivery: cargo-loading functionality based on MnO<sub>2</sub> NSs

As mentioned above, MnO<sub>2</sub> NSs, with extremely large SMRs, exhibit a wide range of distinctive physicochemical properties compared with their bulk composition. One of most typical biomedical applications of MnO<sub>2</sub> NS, is drug delivery due to their large SMRs. Moreover, distinct from conventional drug delivery systems (DDSs), MnO<sub>2</sub> NS-based nanoplatforms can function as controlled or on-demand DDSs. The controlled drug delivery systems (c-DDSs) for current medications have received increasing interest from numerous chemists and

clinical physicians owing to their low toxicities, broad therapeutic windows and ideal administrative efficacies compared with conventional DDSs.<sup>117–121</sup> On-demand DDSs triggered by intrinsic physiological microenvironment changes (eg, pH,<sup>122</sup> redox agents,<sup>123,124</sup> enzymes,<sup>125</sup> and heat<sup>126,127</sup>) and/or external artificially introduced stimuli<sup>128,129</sup> (eg, light,<sup>130</sup> laser pulses,<sup>131</sup> magnetic/electronic fields,<sup>132</sup> and ultrasonication<sup>133</sup>) can simultaneously diminish the side-effects of anticancer agents toward normal tissue to improve the therapeutic effects. Previous reports on DDSs have mainly focused on nanocomposites, such as magnetic composites and upconversion nanoparticles, and most of them have been magnetically functionalized mesoporous materials or hollow spherical particles with the drugs being released via changes in the pH or temperature.<sup>121,134–137</sup> For the use of MnO<sub>2</sub> NSs as controlled drug delivery nanocarriers, two main

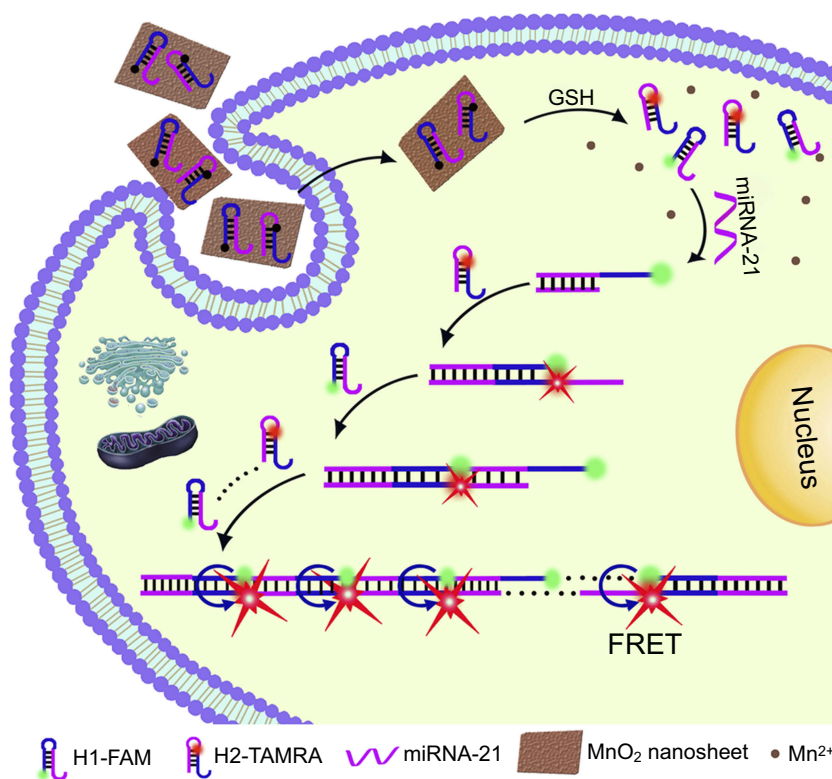


**Figure 6** Schematic illustration of the MnO<sub>2</sub> NS-mediated intracellular-hybridized chain reaction (HCR) signal amplification system for efficiently detecting miRNA-21 in living HeLa cells. The MnO<sub>2</sub> NSs could deliver two types of hairpin DNA probes into the cytosol. Overexpressed glutathione (GSH) in HeLa cells and displacement reactions by other proteins or nucleic acids promoted the decomposition of the MnO<sub>2</sub> NSs to release free hairpins, which assembled into double-stranded (dsDNA) polymers upon binding to the target miRNA-21. Subsequently, enhanced FRET signals were produced to realize accurate and sensitive detection. Reprinted with permission from Li J, Li D, Yuan R, Xiang Y. Biodegradable MnO<sub>2</sub> nanosheet-mediated signal amplification in living cells enables sensitive detection of down-regulated intracellular MicroRNA. *ACS Appl Mater Interfaces*. 2017;9(7):5717–5724.<sup>111</sup> Copyright 2017 American Chemical Society.

properties are beneficial: a large specific surface area and a sensitive response to the tumor microenvironment. In 2013, Zhao et al proposed a novel and facile strategy for the fabrication of multifunctional nanocomposites with silica-coated Fe<sub>2</sub>O<sub>3</sub> particle cores and NaYF<sub>4</sub>:Yb, Er shells, on which MnO<sub>2</sub> NSs were further grown for delivery and release of a model drug, Congo red (CR). In this nanosystem, the MnO<sub>2</sub> NSs served not only as carriers for the loading and release of CR *in vitro* but also as efficient quenchers for the UC luminescence to monitor intracellular GSH concentration (Figure 7).<sup>138</sup> The drug was released upon reduction of MnO<sub>2</sub> to Mn<sup>2+</sup> by GSH, while simultaneously increasing the UC luminescence. The fabricated nanocomposite is a promising platform due to its GSH-stimulated smart drug delivery and UC luminescence monitoring. Indeed, the nanocarrier functionality of MnO<sub>2</sub> NSs has rarely been applied individually and has always been combined with other pragmatic components, eg, fluorescence quenchers and magnetic resonance imaging (MRI) probes, which will be mentioned below.

### As an MRI pro-contrast agent: stimuli-activated imaging based on MnO<sub>2</sub> NSs

MRI was originally known as nuclear magnetic resonance (NMR)<sup>139</sup> imaging and belongs to a configuration of NMR, albeit the “nuclear” employed in the acronym was omitted to avoid negative associations with the word. Certain atomic nuclei are capable of absorbing and releasing radiofrequency (RF) energy in the presence of an external magnetic field. Hydrogen atoms are typically applied to boost the detectable RF signals which can be received by antennas in proximity to the corresponding anatomy for examination. By altering the parameters of the pulse sequence, different degrees of contrast may be generated between tissues based on the relaxation properties of their hydrogen atoms.<sup>140,141</sup> Compared with other imaging modalities, the main advantage of MRI is its superb spatial resolution whereas its major drawback is the limited sensitivity. As such, chemistry and materials science research has focused on searching for solutions capable of solving this challenging hurdle.<sup>142</sup> The introduction of contrast

Table 2 Fluorescent biosensors based on MnO<sub>2</sub> NSs

Nanomaterials	Targets	Linear response concentration	Limit of detection (LOD)	Reference
CDs-MnO <sub>2</sub> NS architecture	GSH	0.2–600 μM	22 nM	86
CDs-MnO <sub>2</sub> nanocomposite	ALP	1–100 U/L	0.4 U/L	85
CQDs-MnO <sub>2</sub> nanocomposite	GSH	0.01–200 μM	0.01 μM	170
GQDs-MnO <sub>2</sub> nanoplatform	GSH	0.5–10 μM	150 nM	87
g-C <sub>3</sub> N <sub>4</sub> -MnO <sub>2</sub> nanosandwich	GSH	200–500 μM	N/A	151
MnO <sub>2</sub> NS-UCP nanosystem	GSH and H <sub>2</sub> O <sub>2</sub>	0–250 and 250–400 μM	3.7 μM	88
MnO <sub>2</sub> NS-UCP nanosystem	L-lactic acid	50–400 and 450–800 μM	10 μM	88
MnO <sub>2</sub> NS-FAM +TMR hairpins	miRNA-21	100–250 nM	100 nM	111
MnO <sub>2</sub> NS label-free platform	Mercury(II) (Hg <sup>2+</sup> )	0–20 n M	0.8 nM	112
MnO <sub>2</sub> NS label-free platform	Ochratoxin (OTA)	0.02–2 nM	0.02 ng/mL	113
MnO <sub>2</sub> NS label-free platform	Cathepsin (Cat D)	1–100 ng/mL	N/A	113
MnO <sub>2</sub> NS-7-hydroxycoumarin	Ascorbic acid	0.5–40 μM	0.09 μM	114
MnO <sub>2</sub> NS-7-hydroxycoumarin	GSH	1–25 μM	300 nM	68
MnO <sub>2</sub> NS & ligand-DNA FP	Silver ions (Ag <sup>+</sup> )	30–240 nM	9.1 nM	115
Ru(BPY) <sub>3</sub> @MnO <sub>2</sub> nanoprobe	GSH	0–300 μM	420 nM	157
MSNs-G@MnO <sub>2</sub> NSs	GSH	100 nM to 10 μM	34 nM	116
MnO <sub>2</sub> NS-cascade logic circuit	GSH	20–2,000 nM	6.7 nM	152

Abbreviations: CD, carbon dot; GSH, glutathione; NS, nanosheet; GQD, graphene quantum dot.

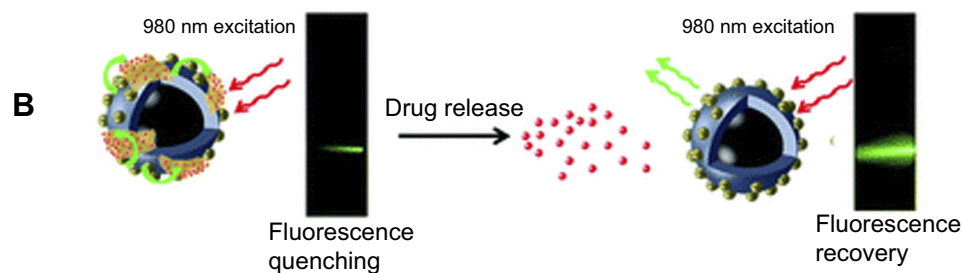
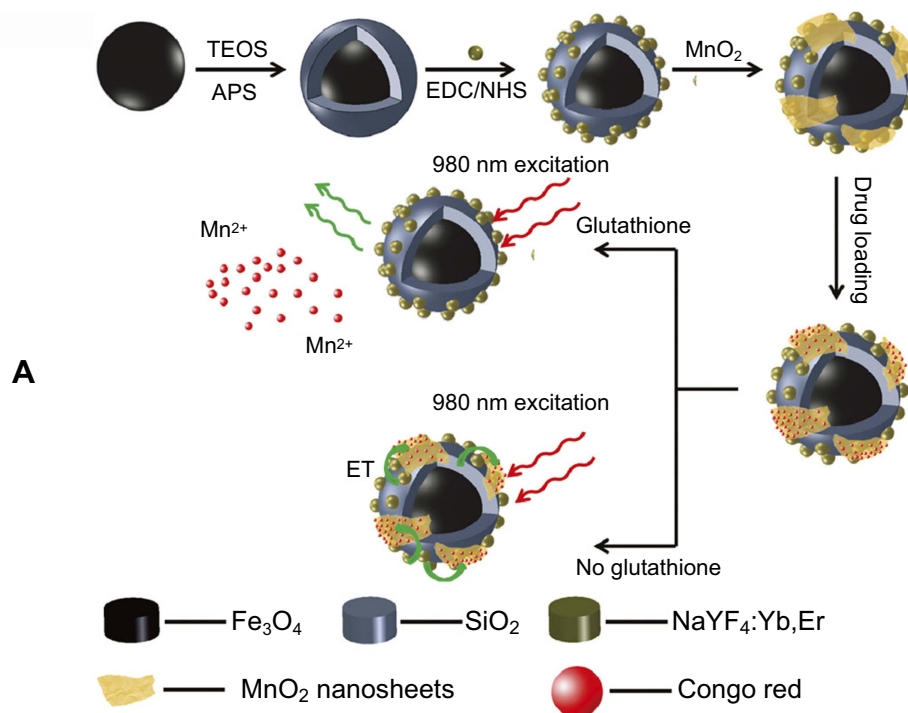


**Figure 7** (A) Schematic illustration of the synthetic procedure for the preparation of the MSU/MnO<sub>2</sub>-CR drug delivery system. (B) Images of the MSU/MnO<sub>2</sub>-CR system before and after drug delivery under 980 nm excitation. Republished with permission of Royal Society of Chemistry, from Multifunctional MnO<sub>2</sub> nanosheet-modified Fe<sub>3</sub>O<sub>4</sub>@SiO<sub>2</sub>/NaYF<sub>4</sub>:yb,Er nanocomposites as novel drug carriers, Zhao P, Zhu Y, Yang X, et al, 43, 2, 2014; permission conveyed through Copyright Clearance Centre, Inc.<sup>138</sup>

agents (CAs) has been the main solution. Paramagnetic complexes comprising metal ions with symmetric electronic ground states, eg, gadolinium (Gd<sup>3+</sup>)<sup>143</sup> and manganese (Mn<sup>2+</sup>),<sup>144</sup> have been successfully applied as MRI CAs since the late 1980s<sup>145</sup> in virtue of their outstanding capabilities to decrease the longitudinal relaxation time T<sub>1</sub> of water protons dipolarly interacting with the unpaired electrons of the metal ions. Manganese-based oxides have been demonstrated as alternative CAs for T<sub>1</sub>-weighted MRI, with relatively improved biocompatibilities and cytotoxicities, to replace the clinically widespread gadolinium-based CAs, which have been warned by US Food and Drug Administration (FDA) due to the correlation between gadolinium and nephrogenic systemic fibrosis, kidney dysfunction, etc.<sup>146–149</sup> The Mn

atoms in MnO<sub>2</sub> nanosheets are coordinated in an octahedral geometry to six oxygen atoms and shielded from aqueous environments, making no contribution to the longitudinal or transverse relaxation of the protons.<sup>150</sup> As Zhang and co-workers reported, the relaxation rate (r<sub>1</sub> value) of initial PEG-MnO<sub>2</sub> NSs was very low (0.007 mM<sup>-1</sup> s<sup>-1</sup>), which was ascribed to the high valence (IV) of manganese and the shielded paramagnetic centers being inaccessible to water molecules.<sup>151</sup> Upon disintegration and degradation, the released Mn<sup>2+</sup> gives rise to a highly improved T<sub>1</sub>-MRI performance because of the five unpaired 3d electrons and the enhanced accessibility of the paramagnetic centers to the surrounding water molecules. As illustrated by Zhang et al, the longitudinal relaxivity r<sub>1</sub> and transverse relaxivity r<sub>2</sub>,

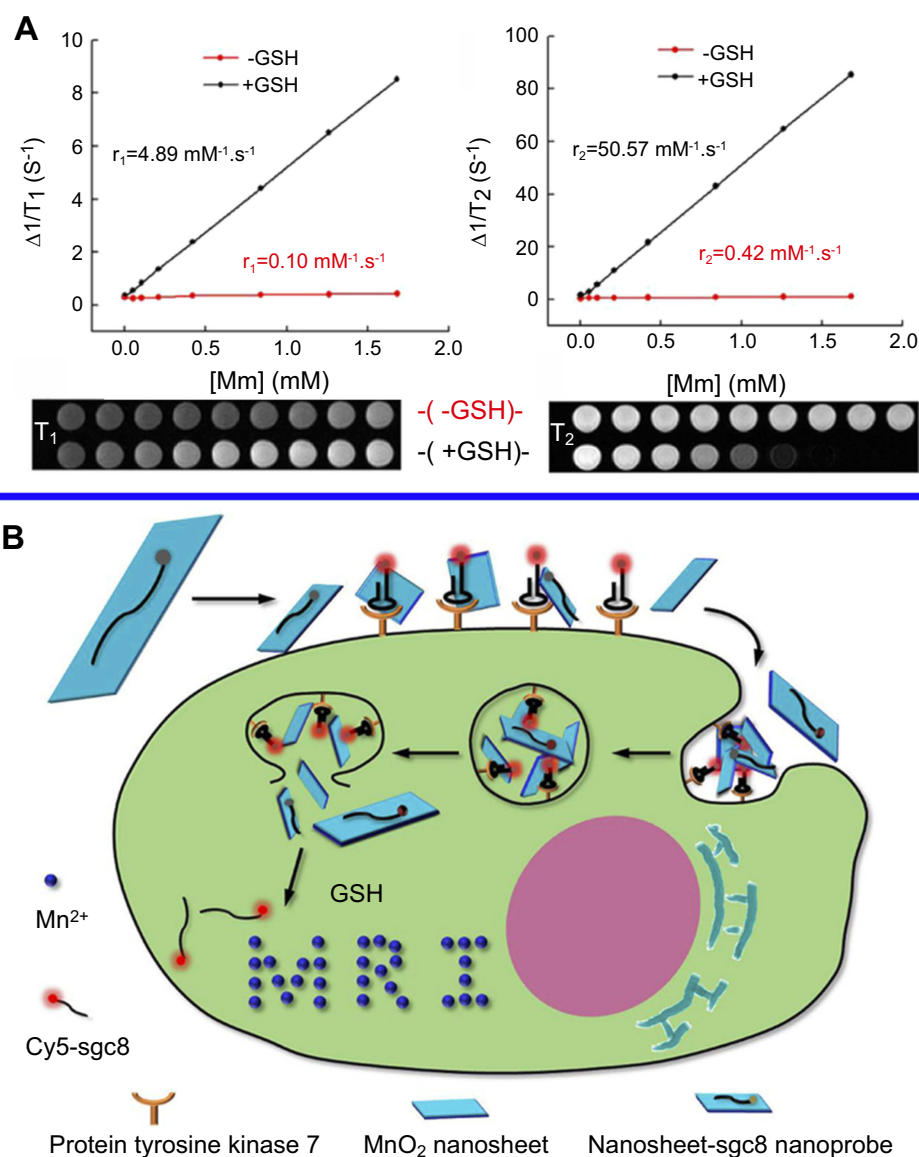


**Figure 8 (A)** Determination of the T<sub>1</sub> (left) and T<sub>2</sub> (right) relaxation rates of a MnO<sub>2</sub> nanosheet solution (red lines) and MnO<sub>2</sub> nanosheet solution treated with GSH (black lines). The related T<sub>1</sub>-weighted and T<sub>2</sub>-weighted MRI images were presented below. **(B)** Schematic illustration of the activation mechanism of the MnO<sub>2</sub> NS-aptamer nanoprobe for fluorescence/MRI bimodal tumor cell imaging. Reprinted with permission from Zhao Z, Fan H, Zhou G, et al. Activatable fluorescence/MRI bimodal platform for tumor cell imaging via MnO<sub>2</sub> nanosheet-aptamer nanoprobe. *J Am Chem Soc.* 2014;136(32):11220–11223.<sup>150</sup> Copyright 2014 American Chemical Society.

obtained by measuring the relaxation rate as a function of Mn concentration, exhibited a 48- (from 0.1 to 4.89 mM<sup>-1</sup> s<sup>-1</sup>) and 120-fold (from 0.42 to 50.57 mM<sup>-1</sup> s<sup>-1</sup>) enhancement, respectively, when the MnO<sub>2</sub> NSs were reduced to Mn<sup>2+</sup> by GSH (Figure 8A).<sup>150</sup> The decomposition of MnO<sub>2</sub> NSs in the tumor microenvironment (GSH-activated<sup>152,153</sup> or pH-dependent<sup>154,155</sup>) to release Mn<sup>2+</sup> can be utilized for tumor cell MR imaging. Wang and Shi's group in 2014, presented an intriguing achievement with their report on an intelligent theranostic platform based on highly disperse 2D MnO<sub>2</sub> NSs for concurrent ultrasensitive pH-responsive MRI and drug delivery/release.<sup>156</sup>

In addition to MRI, MnO<sub>2</sub> NSs have shown promising potential for the fabrication of dual-activatable fluorescence/MRI bimodal platforms. In 2014, Tan and coworkers designed a redox-capable MnO<sub>2</sub> NS-aptamer nanoprobe for multimodal imaging of tumor cells (Figure 8B).<sup>150</sup> In this platform, the MnO<sub>2</sub> NSs played three roles as a DNA nanocarrier, fluorescence quencher and intracellular GSH-activated MRI CA. Upon encountering the target cells, the binding of the aptamer to the corresponding target weakened the absorption of the probe on the NSs and produced a fluorescence recovery as well as aptamer-mediated endocytosis. The intracellular GSH further reduced the MnO<sub>2</sub>

NSs into a large amount of  $Mn^{2+}$  suitable for MRI. Using a similar principle, a  $MnO_2$  NS-Ru(II) complex nanoarchitecture,  $Ru(BYP)_3@MnO_2$  ( $BYP = 2,2'$ -bipyridine) has also been developed for determining GSH in vitro and in vivo.<sup>157</sup>

Despite the multimodal imaging applications of  $MnO_2$  NSs in conjunction with their fluorescence and MR imaging, many exploits have been attempted to accomplish theranostic applications (ie, imaging and killing at the same time). Notably, the PEG- $MnO_2$  NSs reported by Wang and colleagues in 2014 promoted ultrasensitive pH-triggered concurrent diagnostic and therapeutic functionalities (designated as theranostics) for cancers, which provided a novel and facile platform for concurrent ultrasensitive pH-stimulated  $T_1$ -weighted MRI and anti-tumor drug (doxorubicin, Dox) release (Figure 9).<sup>156</sup> The pH-triggered rapid decomposition of 2D  $MnO_2$  NSs in a mildly acidic microenvironment could facilitate the controlled release of delivered anticancer agents and circumvent the multidrug resistance of cancer cells by bypassing the typical P-glycoprotein (P-gp)-induced efflux process with  $MnO_2$  NSs due to their larger size than free Dox molecules.<sup>158</sup>

$MnO_2$  NSs themselves can be used not only as nanocarriers for drug delivery, but also as therapy agents. Recently, Xiaoyuan Chen and colleagues at the National Institute of Health (NIH) reported that the construction of  $MnO_2$ -based nanoagents can augment the efficiency of CDT (Figure 10).<sup>21</sup> CDT utilizes iron-initiated Fenton chemistry to kill tumor cells via the conversion of endogenous  $H_2O_2$  into hydroxyl radicals ( $\cdot OH$ ), which have a high toxicity, inducing intracellular oxidative stress.<sup>159–162</sup> To date, a number of iron-carrying nanoparticles have been employed as CDT agents to induce ferroptosis<sup>163</sup> in tumor cells via  $H_2O_2$ -dependent Fenton-like reaction.<sup>164–167</sup> As envisaged, the overproduction of GSH in tumor cells ought to be one of the most formidable hurdles for the CDT effect in that GSH serves as a scavenger of the highly reactive  $\cdot OH$  generated by chemodynamic agents, thereby increasing the resistance of cancer cells to oxidative stress and diminishing the efficacy of CDT.<sup>168,169</sup> Chen et al was the first time to report that  $MnO_2$ , which possesses both Fenton-like  $Mn^{2+}$  delivery and GSH depletion capabilities, could play a role as a novel chemodynamic agent in order to improve the CDT of cancer via simultaneously disrupting the antioxidant system and loading an  $\cdot OH$  generator into cells. Ultimately, they utilized  $MnO_2$  NSs to successfully construct an activatable theranostic nanosystem for an MRI-monitored chemodynamic combination regimen.<sup>21</sup>

In conclusion, as an MRI CA,  $MnO_2$  NSs can produce an activatable MRI signal upon the degradation of their structure in the tumor microenvironment, favoring the improvement of the signal-to-noise ratio and specificity. Additionally, benefitting from the high surface area, fluorescence quenching ability and CDT ability of  $MnO_2$  NSs, MRI-based theranostic platforms and multimodal imaging nanoprobe can be easily fabricated with the help of  $MnO_2$  NSs, which undoubtedly broadens the applications of MRI.

Taken together,  $MnO_2$  NSs have displayed promising potential in multiple modalities for the diagnosis, treatment and theranostics of tumors in vitro and in vivo.

## Toxicity evaluation of $MnO_2$ nanosheets ( $MnO_2$ NSs)

With the widespread use of  $MnO_2$  NSs in a range of biomedical applications, their toxicological assessment both in vitro and in vivo is extremely important. Nonetheless, there are still a limited number of toxicity studies on  $MnO_2$  NSs especially in vivo. MTT assays and cell counting kit-8 (CCK-8) assays are two commonly employed methods to assess the toxicity of  $MnO_2$  NSs in various cells. Herein, we present the main cytotoxicity testing results of various nanomaterials based on  $MnO_2$  NSs. He et al developed a single-layer  $MnO_2$  NS-quenched fluorescent carbon quantum dots, and their nanosystem exhibited no apparent cytotoxicity at the concentrations of 30  $\mu g/mL$  or less when exposed to HeLa human cervical carcinoma cells for 24 hrs.<sup>170</sup> Similarly Yan et al reported of GQD- $MnO_2$  NS based optical sensing nanoplat-form and confirmed that this nanomaterial had low toxicity even at a concentration of 40  $\mu g/mL$ , toward MCF-7 breast adenocarcinoma cells.<sup>87</sup> Zhang et al have reported that their graphitic- $C_3N_4$ NS- $MnO_2$  sandwich-like nanocomposite displayed no apparent loss in cell viability even at a 50  $\mu g/mL$  exposure to HeLa cells.<sup>151</sup> Recently, corresponding cytotoxicological assessments of  $MnO_2$  NS-based nanosystems in HeLa and MCF-7 cells were carried out by the Xiang group,<sup>111</sup> Chen and coworkers<sup>69</sup> and Shi and colleagues.<sup>157</sup> They all reported excellent biocompatibilities and insignificant viability losses as listed in Table 3. It is also remarkable that the effort of Zhao et al to fabricate  $MnO_2$  NS-aptamer nanoprobe early in 2014 verified that 79% of CCRF-CEM and Ramos human B lymphoma cells remained alive following by exposure to their nanoprobe at a concentration of 1 mM for 24 hrs.<sup>150</sup>

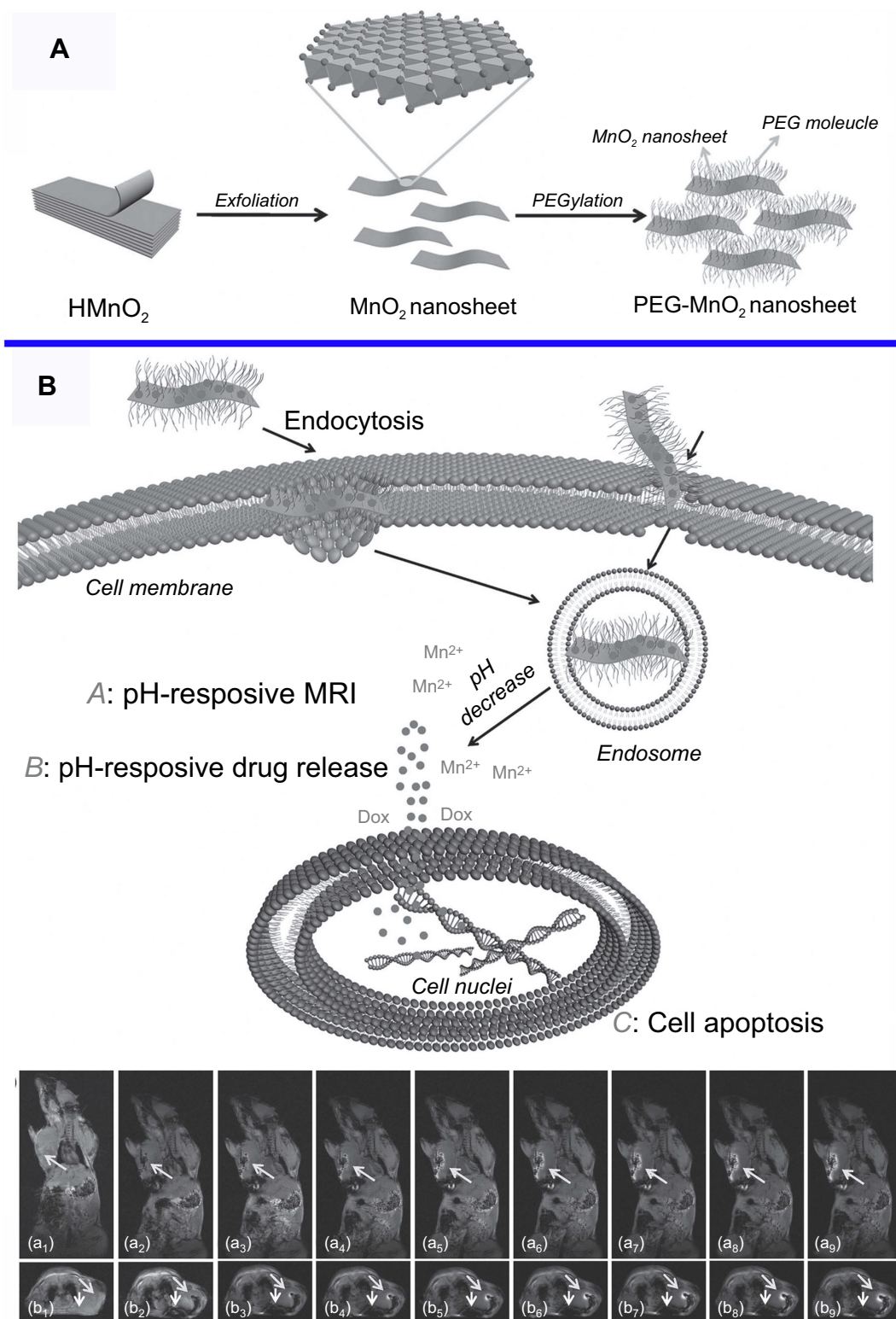


**Figure 9** (A) Schematic illustration of the synthetic procedure for the PEG-MnO<sub>2</sub> NSs. (B) Theranostic functionality of the PEG-MnO<sub>2</sub> NSs for intracellular pH-responsive drug release and the axial and coronal T<sub>1</sub>-MRI images of 4T1 tumor-bearing nude mice before (a<sub>1</sub>, b<sub>1</sub>) and after (a<sub>2</sub> – a<sub>9</sub> and b<sub>2</sub> – b<sub>9</sub>) administration of the PEG-MnO<sub>2</sub> nanosheets within the tumor and normal subcutaneous tissue. PEG denotes ethylene glycol. Reproduced with permission from Chen Y, Ye D, Wu M, et al. Break-up of two-dimensional MnO<sub>2</sub> nanosheets promotes ultrasensitive pH-triggered theranostics of cancer. *Adv Mater Weinheim*. 2014;26(41):7019–7026. <sup>156</sup> Copyright © 2014, John Wiley and Sons.

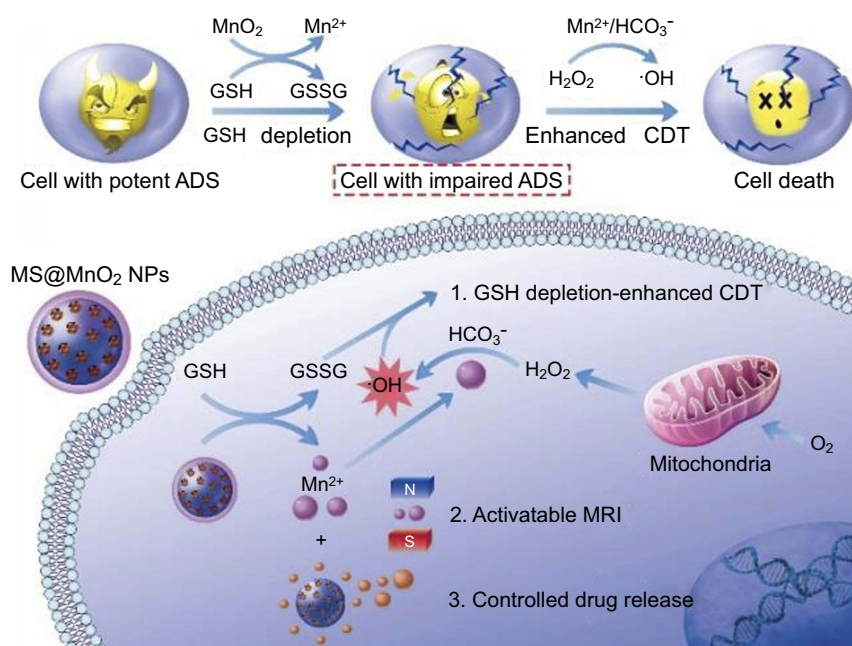


**Figure 10** Schematic illustrations of the mechanism and application of mesoporous silicon (MS)@MnO<sub>2</sub> NPs for MRI-monitored chemo-chemodynamic combination therapy. Reproduced with permission from Lin L, Song J, Song L, et al. Simultaneous fenton-like ion delivery and glutathione depletion by MnO<sub>2</sub>-based nanoagent to enhance chemodynamic therapy. *Angew Chem Int Ed Engl.* 2018;57(18):4902–4906.<sup>21</sup> Copyright © 2018, John Wiley and Sons.

## Conclusion and perspectives

Over the last few decades, research on the synthesis and biomedical applications of MnO<sub>2</sub> NSs has thrived and seen impressive advancements. In this review, first of all, we highlighted the state-of-the-art strategies that have been developed for the preparation of MnO<sub>2</sub> NSs by top-down or bottom-up methods. Notwithstanding, in contrast to other 2D nanomaterials, the top-down approach of MnO<sub>2</sub> NS synthesis is obviously costly and time-consuming. Moreover, it is fairly difficult to completely exfoliate the protonated compounds completely into single-layer NSs (monosheets), thus, previously obtained NSs have always had a wide thickness distribution in practice. The bottom-up strategies, comprising the oxidative and the reductive methods, have been widely utilized widespread. MnO<sub>2</sub> NSs can be facilely prepared via the reduction of KMnO<sub>4</sub> in the presence of an MES buffer at pH 6 or through the oxidation of MnCl<sub>2</sub> with oxidants, eg, H<sub>2</sub>O<sub>2</sub> in the coexistence of TMA·OH as summarized above. Numerous reductants can be selected, and the synthetic process for MnO<sub>2</sub> NSs is tunable. Although many intriguing methods have been developed in this inspiring research field, it is still urgent to develop new facile and effective methods for the synthesis of high-quality MnO<sub>2</sub> NSs.

Then, we provided an overview of the main applications of MnO<sub>2</sub> NSs in biomedicine. MnO<sub>2</sub> NSs can play multiple roles as nanozymes, nanocargos, fluorescence quenchers and activatable MRI probes. Hitherto, almost all of the reported biomedical applications have been based on these four fundamental functionalities and their roles are not dichotomies towards each other. Numerous researchers have focused on integrating MnO<sub>2</sub> NSs into multiple modalities to explore increasingly novel uses in biomedicine.

Last but not the least, biosafety is one of the most concerning issues for the use of nanomaterials in biomedical employments before end-point clinical translation, despite the knowledge of the toxicity for MnO<sub>2</sub> NSs are still very preliminary and limited. Therefore, the toxicity of MnO<sub>2</sub> NSs should be systematically and comprehensively validated, especially in vivo. In addition, several intermediate metabolites accumulate in living organisms and cannot be easily degraded or detoxified, resulting in long-term toxicity issues, which should be further considered.

In the future, for MnO<sub>2</sub> NS-related research, the biosafety should be considered first. Thus, green synthetic approaches are preferred for obtaining MnO<sub>2</sub> NSs with controllable thicknesses, sizes and morphologies. The biomedical applications of MnO<sub>2</sub> NSs have experienced markedly rapid advancement over the last few

Table 3 Cytotoxicity results of various nanomaterials based on MnO<sub>2</sub> NSs

Nanomaterials	Cell lines	Response, maximum exposure concentration, and duration	Testing assays	Reference
CQDs-MnO <sub>2</sub> NS	Hela	No apparent loss of cell viability, 30 µg/mL, 24 hrs	MTT	170
GQDs-MnO <sub>2</sub> nanoprobe	MCF-7	Low cytotoxicity, 40 µg/mL, 24 hrs	MTT	87
g-C <sub>3</sub> N <sub>4</sub> -MnO <sub>2</sub> nanosandwich	Hela	No apparent loss of cell viability, 50 µg/mL, 24 hrs	CCK-8	151
MnO <sub>2</sub> NS-FAM + TMR hairpins	Hela	Insignificant viability loss, 86% alive, 60 µg/mL, 24 hrs	MTT	111
MnO <sub>2</sub> NS-FAM + TMR hairpins	MCF-7 & HepG2	Low cytotoxicity, 90 µg/mL, 24 hrs	MTT	171
MnO <sub>2</sub> NS-janus DNA machine	MCF-7	Good biocompatibility, 100 µg/mL, 24 hrs	MTT	69
MnO <sub>2</sub> NS-apptamer nanoprobe	CCRF-CEM and Ramos	79% of cells remained alive, 1 mM, 24 hrs	MTS	150
Ru(BPY) <sub>3</sub> @MnO <sub>2</sub> nanoprobe	Hela	The viabilities remained higher than 87%, 160 µM, 24 hrs	MTT	157
MnO <sub>2</sub> NS-"DD-A" binary probe	HepG2	Low cytotoxicity, 90 µg/mL, 24 hrs	MTT	172

Abbreviations: CCK-8, cell counting kit-8; NS, nanosheet; GQD, graphene quantum dot.

decades. However, the targets are relatively limited. Extra attention should be paid to integrating proper targeting aptamers/antigens/antibodies especially those that play important roles in cancer cell signaling pathways with MnO<sub>2</sub> NSs. This will help to improve both the performance of biosensors and the efficacy of cancer theranostics based on MnO<sub>2</sub> NSs. Furthermore, additional applications of MnO<sub>2</sub> NSs such as PTT and imaging-guided combination therapy, should be considered to broaden their biomedical applications. As envisaged optimistically, the MnO<sub>2</sub> NSs will provide promising opportunities for the realization of more advanced medical imaging. We also believe that this review may entice other scientists in multiple disciplines to join into this new but growing research field.

## Acknowledgments

This work was supported by the National Natural Science Foundation of China (81771904, 81502280), the Natural Science Foundation of Jiangsu Province for the Excellent Young Scholars (BK20170054), China Postdoctoral Science Foundation (2016M601890, 177607), Qing Lan Project, the Peak of Six Talents of Jiangsu Province (WSN-112), Jiangsu Provincial Medical Youth Talent (QNRC2016776), Six One Project of Jiangsu Province (LGY2018083) and Postgraduate Research & Practice Innovation Program of Jiangsu Province (SJCX18\_0708).

## Disclosure

The authors report no conflicts of interest in this work.

## References

- Mansouri A, Gattolliat C, Asselah T. Mitochondrial dysfunction and signaling in chronic liver diseases. *Gastroenterology*. 2018;155:629–647. doi:10.1053/j.gastro.2018.06.083
- Fruman D, Chiu H, Hopkins B, Bagrodia S, Cantley L, Abraham R. The PI3K pathway in human disease. *Cell*. 2017;170(4):605–635. doi:10.1016/j.cell.2017.07.029
- McInnes I, Schett G. Pathogenetic insights from the treatment of rheumatoid arthritis. *Lancet*. 2017;389(10086):2328–2337. doi:10.1016/S0140-6736(17)31472-1
- Nusse R, Clevers H. Wnt/β-catenin signaling, disease, and emerging therapeutic modalities. *Cell*. 2017;169(6):985–999. doi:10.1016/j.cell.2017.05.016
- Wang Q, Kalantar-Zadeh K, Kis A, Coleman J, Strano M. Electronics and optoelectronics of two-dimensional transition metal dichalcogenides. *Nat Nanotechnol*. 2012;7(11):699–712.
- Meyer J, Hamwi S, Kröger M, Kowalsky W, Riedl T, Kahn A. Transition metal oxides for organic electronics: energetics, device physics and applications. *Adv Mater Weinheim*. 2012;24(40):5408–5427.

7. Loh K, Ho D, Chiu G, Leong D, Pastorin G, Chow E. Clinical applications of carbon nanomaterials in diagnostics and therapy. *Adv Mater Weinheim*. 2018;30(47):e1802368.
8. Wu W, Qiu G, Wang Y, Wang R, Ye P. Tellurene: its physical properties, scalable nanomanufacturing, and device applications. *Chem Soc Rev*. 2018;47:7203–7212.
9. Chimene D, Alge D, Gaharwar A. Two-dimensional nanomaterials for biomedical applications: emerging trends and future prospects. *Adv Mater Weinheim*. 2015;27(45):7261–7284.
10. Veeramani H, Aruguete D, Monsegue N, et al. Low-temperature green synthesis of multivalent manganese oxide nanowires. *ACS Sustain Chem Eng*. 2013;1(1070–1074).
11. Layfield RA. Manganese(II): the black sheep of the organometallic family. *Chem Soc Rev*. 2008;37(6):1098–1107. doi:10.1039/b708850g
12. Fei J, Cui Y, Yan X, et al. Controlled preparation of MnO<sub>2</sub> hierarchical hollow nanostructures and their application in water treatment. *Adv Mater*. 2008;20:452–456. doi:10.1002/adma.200701231
13. Prasad AS. Green synthesis of nanocrystalline manganese (II, III) oxide. *Mater Sci Semicond Process*. 2017;71:342–347. doi:10.1016/j.mssp.2017.08.020
14. Hoseinpour V, Ghaemi N. Green synthesis of manganese nanoparticles: applications and future perspective-A review. *J Photochem Photobiol B*. 2018;189(undef):234–243. doi:10.1016/j.jphotobiol.2018.10.022
15. Guo S, Dong S. Graphene nanosheet: synthesis, molecular engineering, thin film, hybrids, and energy and analytical applications. *Chem Soc Rev*. 2011;40(5):2644–2672. doi:10.1039/c0cs00079e
16. Zhao M, Huang Y, Peng Y, Huang Z, Ma Q, Zhang H. Two-dimensional metal-organic framework nanosheets: synthesis and applications. *Chem Soc Rev*. 2018;47(16):6267–6295. doi:10.1039/c8cs00268a
17. Li X, Shan J, Zhang W, Su S, Yuwen L, Wang L. Recent advances in synthesis and biomedical applications of two-dimensional transition metal dichalcogenide nanosheets. *Small*. 2017;13(5):1602660. doi:10.1002/sml.13.5
18. Wang H, Zhang J, Hang X, et al. Half-metallicity in single-layered manganese dioxide nanosheets by defect engineering. *Angew Chem Int Ed Engl*. 2015;54(4):1195–1199. doi:10.1002/anie.201410031
19. Rani A, Velusamy D, Kim R, et al. Non-volatile ReRAM devices based on self-assembled multilayers of modified graphene oxide 2D nanosheets. *Small*. 2016;12(44):6167–6174. doi:10.1002/sml.201602276
20. Fan H, Yan G, Zhao Z, et al. A smart photosensitizer-manganese dioxide nanosystem for enhanced photodynamic therapy by reducing glutathione levels in cancer cells. *Angew Chem Int Ed Engl*. 2016;55(18):5477–5482. doi:10.1002/anie.201510748
21. Lin L, Song J, Song L, et al. Simultaneous fenton-like ion delivery and glutathione depletion by MnO<sub>2</sub>-based nanoagent to enhance chemodynamic therapy. *Angew Chem Int Ed Engl*. 2018;57(18):4902–4906. doi:10.1002/anie.201712027
22. Xu Y, Chen X, Chai R, Xing C, Li H, Yin X. A magnetic/fluorometric bimodal sensor based on a carbon dots-MnO<sub>2</sub> platform for glutathione detection. *Nanoscale*. 2016;8(27):13414–13421. doi:10.1039/c6nr03129c
23. Lhuillier E, Pedetti S, Ithurria S, Nadal B, Heuclin H, Dubertret B. Two-dimensional colloidal metal chalcogenides semiconductors: synthesis, spectroscopy, and applications. *Acc Chem Res*. 2015;48(1):22–30. doi:10.1021/ar500326c
24. Omomo Y, Sasaki T, Wang L, Watanabe M. Redoxable nanosheet crystallites of MnO<sub>2</sub> derived via delamination of a layered manganese oxide. *J Am Chem Soc*. 2003;125(12):3568–3575. doi:10.1021/ja021364p
25. Kai K, Yoshida Y, Kageyama H, et al. Room-temperature synthesis of manganese oxide monosheets. *J Am Chem Soc*. 2008;130(47):15938–15943. doi:10.1021/ja804503f
26. Tae E, Lee K, Jeong J, Yoon K. Synthesis of diamond-shape titanate molecular sheets with different sizes and realization of quantum confinement effect during dimensionality reduction from two to zero. *J Am Chem Soc*. 2008;130(20):6534–6543. doi:10.1021/ja711467g
27. Oaki Y, Imai H. One-pot synthesis of manganese oxide nanosheets in aqueous solution: chelation-mediated parallel control of reaction and morphology. *Angew Chem Int Ed Engl*. 2007;46(26):4951–4955. doi:10.1002/anie.200700244
28. Deng R, Xie X, Vendrell M, Chang Y, Liu X. Intracellular glutathione detection using MnO(2)-nanosheet-modified upconversion nanoparticles. *J Am Chem Soc*. 2011;133(50):20168–20171. doi:10.1021/ja2100774
29. Liu Z, Xu K, Sun H, Yin S. One-step synthesis of single-layer MnO<sub>2</sub> nanosheets with multi-role sodium dodecyl sulfate for high-performance pseudocapacitors. *Small*. 2015;11(18):2182–2191. doi:10.1002/sml.201402222
30. Peng J, Dong M, Ran B, et al. “One-for-All”-type, biodegradable prussian blue/manganese dioxide hybrid nanocrystal for trimodal imaging-guided photothermal therapy and oxygen regulation of breast cancer. *ACS Appl Mater Interfaces*. 2017;9(16):13875–13886. doi:10.1021/acsami.7b01365
31. Meng X, Lu L, Sun C. Green synthesis of three-dimensional MnO/graphene hydrogel composites as a high-performance electrode material for supercapacitors. *ACS Appl Mater Interfaces*. 2018;10(19):16474–16481. doi:10.1021/acsami.8b02354
32. Zhang Y, Wang F, Ou P, et al. High efficiency and rapid degradation of bisphenol A by the synergy between adsorption and oxidization on the MnO@nano hollow carbon sphere. *J Hazard Mater*. 2018;360:223–232. doi:10.1016/j.jhazmat.2018.08.003
33. Lu X, Shen C, Zhang Z, Barrios E, Zhai L. Core-shell composite fibers for high-performance flexible supercapacitor electrodes. *ACS Appl Mater Interfaces*. 2018;10(4):4041–4049. doi:10.1021/acsami.7b12997
34. Borysiewicz M, Ekielski M, Ogorzałek Z, Wzorek M, Kaczmarski J, Wojciechowski T. Highly transparent supercapacitors based on ZnO/MnO nanostructures. *Nanoscale*. 2017;9(22):7577–7587. doi:10.1039/c7nr01320e
35. Peng X, Guo Y, Yin Q, et al. Double-exchange effect in two-dimensional MnO nanomaterials. *J Am Chem Soc*. 2017;139:5242–5248. doi:10.1021/jacs.7b01903
36. Fan H, Zhao Z, Yan G, et al. A smart DNzyme-MnO(2) nanosystem for efficient gene silencing. *Angew Chem Int Ed Engl*. 2015;54(16):4801–4805. doi:10.1002/anie.201411417
37. Cheng S, Xu C, Deng S, et al. Interface reconstruction with emerging charge ordering in hexagonal manganite. *Sci Adv*. 2018;4(5):eaar4298. doi:10.1126/sciadv.aar4298
38. Zhang J, Zhao Z, Xia Z, Dai L. A metal-free bifunctional electrocatalyst for oxygen reduction and oxygen evolution reactions. *Nat Nanotechnol*. 2015;10(5):444–452. doi:10.1038/nnano.2015.48
39. Cheng F, Shen J, Peng B, Pan Y, Tao Z, Chen J. Rapid room-temperature synthesis of nanocrystalline spinels as oxygen reduction and evolution electrocatalysts. *Nat Chem*. 2011;3(1):79–84. doi:10.1038/nchem.931
40. Xu M, Liang T, Shi M, Chen H. Graphene-like two-dimensional materials. *Chem Rev*. 2013;113(5):3766–3798. doi:10.1021/cr300263a
41. Jia H, Cai Y, Lin J, et al. Heterostructural graphene quantum Dot/MnO nanosheets toward high-potential window electrodes for high-performance supercapacitors. *Adv Sci (Weinh)*. 2018;5(5):1700887. doi:10.1002/advs.201700887

42. Zhang JS, Zhang YZ, Tao J, Sun YY, Zhu YN. Preparation and luminescent properties of SiO<sub>2</sub>-Sr(4)Al(14)O(25): eu<sup>2+</sup>,Dy<sup>3+</sup>/light conversion agent phosphor for anti-counterfeiting application. *J Mater Sci-Mater El.* 2018;29(13):10762–10768. doi:10.1007/s10854-018-9142-9
43. Huang Z, Song Y, Feng D, Sun Z, Sun X, Liu X. High mass loading MnO with hierarchical nanostructures for supercapacitors. *ACS Nano.* 2018;12(4):3557–3567. doi:10.1021/acsnano.8b00621
44. Zhu S, Li L, Liu J, et al. Structural directed growth of ultrathin parallel birnessite on β-MnO for high-performance asymmetric supercapacitors. *ACS Nano.* 2018;12(2):1033–1042. doi:10.1021/acsnano.7b03431
45. Zhai T, Sun S, Liu X, Liang C, Wang G, Xia H. Achieving insertion-like capacity at ultrahigh rate via tunable surface pseudocapacitance. *Adv Mater Weinheim.* 2018;30(12):e1706640.
46. Lee S, Wu L, Poyraz A, et al. Lithiation mechanism of tunnel-structured MnO electrode investigated by in situ transmission electron microscopy. *Adv Mater Weinheim.* 2017;29(43). doi:10.1002/adma.201703186
47. Shen X, Qian T, Zhou J, Xu N, Yang T, Yan C. Highly flexible full lithium batteries with self-knitted α-MnO<sub>2</sub> fabric foam. *ACS Appl Mater Interfaces.* 2015;7(45):25298–25305.
48. Yue Y, Yang Z, Liu N, et al. A flexible integrated system containing a microsupercapacitor, a photodetector, and a wireless charging coil. *ACS Nano.* 2016;10(12):11249–11257.
49. Galbiati M, Barraud C, Tatay S, et al. Unveiling self-assembled monolayers' potential for molecular spintronics: spin transport at high voltage. *Adv Mater Weinheim.* 2012;24(48):6429–6432.
50. Qiu M, Ren W, Jeong T, et al. Omnipotent phosphorene: a next-generation, two-dimensional nanoplatform for multidisciplinary biomedical applications. *Chem Soc Rev.* 2018;47(15):5588–5601.
51. Li Y, Wang Y, Huang G, Gao J. Cooperativity principles in self-assembled nanomedicine. *Chem Rev.* 2018;118(11):5359–5391.
52. Tonga G, Jeong Y, Duncan B, et al. Supramolecular regulation of bioorthogonal catalysis in cells using nanoparticle-embedded transition metal catalysts. *Nat Chem.* 2015;7(7):597–603.
53. Burton A, Thomson A, Dawson W, Brady R, Woolfson D. Installing hydrolytic activity into a completely de novo protein framework. *Nat Chem.* 2016;8(9):837–844.
54. Long L, Liu J, Lu K, et al. Highly sensitive and robust peroxidase-like activity of Au-Pt core/shell nanorod-antigen conjugates for measles virus diagnosis. *J Nanobiotechnology.* 2018;16(1):46–55.
55. Wang H, Li P, Yu D, et al. Unraveling the enzymatic activity of oxygenated carbon nanotubes and their application in the treatment of bacterial infections. *Nano Lett.* 2018;18(6):3344–3351.
56. Fan K, Xi J, Fan L, et al. In vivo guiding nitrogen-doped carbon nanozyme for tumor catalytic therapy. *Nat Commun.* 2018;9(1):1440–1450.
57. Feng L, Dong Z, Liang C, et al. Iridium nanocrystals encapsulated liposomes as near-infrared light controllable nanozymes for enhanced cancer radiotherapy. *Biomaterials.* 2018;181:81–91.
58. Hu Y, Cheng H, Zhao X, et al. Surface-enhanced raman scattering active gold nanoparticles with enzyme-mimicking activities for measuring glucose and lactate in living tissues. *ACS Nano.* 2017;11(6):5558–5566.
59. Li J, Cao Y, Hinman S, et al. Efficient label-free chemiluminescent immunosensor based on dual functional cupric oxide nanorods as peroxidase mimics. *Biosens Bioelectron.* 2018;100:304–311.
60. Nagvenkar A, Gedanken A. Cu<sub>0.89</sub>Zn<sub>0.11</sub>O, A new peroxidase-mimicking nanozyme with high sensitivity for glucose and antioxidant detection. *ACS Appl Mater Interfaces.* 2016;8(34):22301–22308.
61. Qin L, Wang X, Liu Y, Wei H. 2D-metal-organic-framework-nanozyme sensor arrays for probing phosphates and their enzymatic hydrolysis. *Anal Chem.* 2018;90(16):9983–9989.
62. Tao Y, Lin Y, Huang Z, Ren J, Qu X. Incorporating graphene oxide and gold nanoclusters: a synergistic catalyst with surprisingly high peroxidase-like activity over a broad pH range and its application for cancer cell detection. *Adv Mater Weinheim.* 2013;25(18):2594–2599.
63. Hui C, Liu M, Li Y, Brennan J. A paper sensor printed with multifunctional bio/nano materials. *Angew Chem Int Ed Engl.* 2018;57(17):4549–4553.
64. Ouyang H, Tu X, Fu Z, et al. Colorimetric and chemiluminescent dual-readout immunochromatographic assay for detection of pesticide residues utilizing g-CN/BiFeO nanocomposites. *Biosens Bioelectron.* 2018;106:43–49.
65. Wang Z, Dong K, Liu Z, et al. Activation of biologically relevant levels of reactive oxygen species by Au/g-CN hybrid nanozyme for bacteria killing and wound disinfection. *Biomaterials.* 2017;113:145–157.
66. Yin W, Ma D, Yu J, et al. Synthesis of surface modification oriented nano-sized molybdenum disulfide with high peroxidase-like catalytic activity for H<sub>2</sub>O<sub>2</sub> and cholesterol detection. *Chemistry.* 2018;24:15868–15878.
67. Liu X, Wang Q, Zhao H, Zhang L, Su Y, Lv Y. BSA-templated MnO<sub>2</sub> nanoparticles as both peroxidase and oxidase mimics. *Analyst.* 2012;137(19):4552–4558.
68. Liu J, Meng L, Fei Z, Dyson P, Jing X, Liu X. MnO nanosheets as an artificial enzyme to mimic oxidase for rapid and sensitive detection of glutathione. *Biosens Bioelectron.* 2017;90:69–74.
69. Chen F, Bai M, Zhao Y, Cao K, Cao X, Zhao Y. MnO-nanosheet-powered protective janus DNA nanomachines supporting robust RNA imaging. *Anal Chem.* 2018;90(3):2271–2276. doi:10.1021/acs.analchem.7b04634
70. Li J, Cheng F, Huang H, Li L, Zhu J. Nanomaterial-based activatable imaging probes: from design to biological applications. *Chem Soc Rev.* 2015;44(21):7855–7880.
71. Liu Y, Dong X, Chen P. Biological and chemical sensors based on graphene materials. *Chem Soc Rev.* 2012;41(6):2283–2307.
72. Baldo M, Thompson M, Forrest S. High-efficiency fluorescent organic light-emitting devices using a phosphorescent sensitizer. *Nature.* 2000;403(6771):750–753.
73. Prevo B, Peterman E. Förster resonance energy transfer and kinesin motor proteins. *Chem Soc Rev.* 2014;43(4):1144–1155.
74. Puchert R, Steiner F, Plechinger G, et al. Spectral focusing of broadband silver electroluminescence in nanoscopic FRET-LEDs. *Nat Nanotechnol.* 2017;12(7):637–641.
75. Pian Q, Yao R, Sinsuebphon N, Intes X. Compressive hyperspectral time-resolved wide-field fluorescence lifetime imaging. *Nat Photonics.* 2017;11:411–414.
76. Wu Y, Qiu X, Lindbo S, et al. Quantum dot-based FRET immunoassay for HER2 using ultrasmall affinity proteins. *Small.* 2018;14(35):e1802266.
77. Salis F, Descalzo A, Benito-Peña E, Moreno-Bondi M, Orellana G. Highly fluorescent magnetic nanobeads with a remarkable Stokes shift as labels for enhanced detection in immunoassays. *Small.* 2018;14(20):e1703810.
78. Wang H, Li C, Liu X, Zhou X, Wang F. Construction of an enzyme-free concatenated DNA circuit for signal amplification and intracellular imaging. *Chem Sci.* 2018;9(26):5842–5849.
79. Melnychuk N, Klymchenko A. DNA-functionalized dye-loaded polymeric nanoparticles: ultrabright FRET platform for amplified detection of nucleic acids. *J Am Chem Soc.* 2018;140:10856–10865.

80. Huang D, Huang Z, Xiao H, Wu Z, Tang L, Jiang J. Protein scaffolded DNA tetrads enable efficient delivery and ultrasensitive imaging of miRNA through crosslinking hybridization chain reaction. *Chem Sci*. 2018;9(21):4892–4897.
81. Qiu X, Guo J, Jin Z, Petreto A, Medintz I, Hildebrandt N. Multiplexed nucleic acid hybridization assays using single-FRET-pair distance-tuning. *Small*. 2017;13(25):1700332.
82. Teunissen A, Pérez-Medina C, Meijerink A, Mulder W. Investigating supramolecular systems using Förster resonance energy transfer. *Chem Soc Rev*. 2018;47:7027–7044.
83. Dyla M, Terry D, Kjaergaard M, et al. Dynamics of P-type ATPase transport revealed by single-molecule FRET. *Nature*. 2017;551(7680):346–351.
84. Ji C, Lu Z, Xu Y, Shen B, Yu S, Shi D. Self-production of oxygen system CaO/MnO @PDA-MB for the photodynamic therapy research and switch-control tumor cell imaging. *J Biomed Mater Res Part B Appl Biomater*. 2018;106:2544–2552.
85. Qu F, Pei H, Kong R, Zhu S, Xia L. Novel turn-on fluorescent detection of alkaline phosphatase based on green synthesized carbon dots and MnO nanosheets. *Talanta*. 2017;165:136–142.
86. Wang Y, Jiang K, Zhu J, Zhang L, Lin H. A FRET-based carbon dot-MnO<sub>2</sub> nanosheet architecture for glutathione sensing in human whole blood samples. *Chem Commun (Camb)*. 2015;51(64):12748–12751.
87. Yan X, Song Y, Zhu C, et al. Graphene quantum dot-MnO<sub>2</sub> nanosheet based optical sensing platform: a sensitive fluorescence “Turn Off-On” nanosensor for glutathione detection and intracellular imaging. *ACS Appl Mater Interfaces*. 2016;8(34):21990–21996.
88. Yuan J, Cen Y, Kong X, et al. MnO<sub>2</sub>-nanosheet-modified upconversion nanosystem for sensitive turn-on fluorescence detection of H<sub>2</sub>O<sub>2</sub> and glucose in blood. *ACS Appl Mater Interfaces*. 2015;7(19):10548–10555.
89. You J, Jones P. Cancer genetics and epigenetics: two sides of the same coin? *Cancer Cell*. 2012;22(1):9–20.
90. Kasinski A, Slack F. Epigenetics and genetics. MicroRNAs en route to the clinic: progress in validating and targeting microRNAs for cancer therapy. *Nat Rev Cancer*. 2011;11(12):849–864.
91. Esteller M. Non-coding RNAs in human disease. *Nat Rev Genet*. 2011;12(12):861–874.
92. Honkanen S, Thamm A, Arteaga-Vazquez M, Dolan L. Negative regulation of conserved class I bHLH transcription factors evolved independently among land plants. *Elife*. 2018;7:e38529.
93. Chen X, Wang L, Huang R, et al. Dgcr8 deletion in the primitive heart uncovered novel microRNA regulating the balance of cardiac-vascular gene program. *Protein Cell*. 2018;10:327–346.
94. Sun Q, Tripathi V, Yoon J, et al. MIR100 host gene-encoded lncRNAs regulate cell cycle by modulating the interaction between HuR and its target mRNAs. *Nucleic Acids Res*. 2018;46:10405–10416.
95. Cesana M, Guo M, Cacchiarelli D, et al. A CLK3-HMGA2 alternative splicing axis impacts human hematopoietic stem cell molecular identity throughout development. *Cell Stem Cell*. 2018;22(4):575–588.e577.
96. El Harane N, Kervadec A, Bellamy V, et al. Acellular therapeutic approach for heart failure: in vitro production of extracellular vesicles from human cardiovascular progenitors. *Eur Heart J*. 2018;39(20):1835–1847.
97. Esteller M. Epigenetics in cancer. *N Engl J Med*. 2008;358(11):1148–1159. doi:10.1056/NEJMra072067
98. Robertson A, Kim J, Al-Ahmadie H, et al. Comprehensive molecular characterization of muscle-invasive bladder cancer. *Cell*. 2017;171(3):540–556. doi:10.1016/j.cell.2017.09.007
99. Xu R, Rai A, Chen M, Suwakulsiri W, Greening D, Simpson R. Extracellular vesicles in cancer – implications for future improvements in cancer care. *Nat Rev Clin Oncol*. 2018;15:617–638. doi:10.1038/s41571-018-0036-9
100. Ozawa T, Kandimalla R, Gao F, et al. A microRNA signature associated with metastasis of T1 colorectal cancers to lymph nodes. *Gastroenterology*. 2018;154(4):844–848. doi:10.1053/j.gastro.2017.11.275
101. Yu T, Guo F, Yu Y, et al. Fusobacterium nucleatum promotes chemoresistance to colorectal cancer by modulating autophagy. *Cell*. 2017;170(3):548–563. doi:10.1016/j.cell.2017.07.008
102. Hall D, Cost N, Hegde S, et al. TRPM3 and miR-204 establish a regulatory circuit that controls oncogenic autophagy in clear cell renal cell carcinoma. *Cancer Cell*. 2014;26(5):738–753. doi:10.1016/j.ccr.2014.09.015
103. Song Y, Yan X, Ostermeyer G, et al. Direct cytosolic MicroRNA detection using single-layer perfluorinated tungsten diselenide nanoplateform. *Anal Chem*. 2018;90:10369–10376. doi:10.1021/acs.analchem.8b02193
104. Liu C, Chen C, Li S, et al. Target-triggered catalytic hairpin assembly-induced core-satellite nanostructures for high-sensitive “Off-to-On” SERS detection of intracellular microRNA. *Anal Chem*. 2018;90:10591–10599. doi:10.1021/acs.analchem.8b02819
105. Ye S, Wang M, Wang Z, Zhang N, Luo X. A DNA-linker-DNA bifunctional probe for simultaneous SERS detection of miRNAs via symmetric signal amplification. *Chem Commun (Camb)*. 2018;54(56):7786–7789. doi:10.1039/c8cc02910e
106. Dai W, Zhang J, Meng X, et al. Catalytic hairpin assembly gel assay for multiple and sensitive microRNA detection. *Theranostics*. 2018;8(10):2646–2656.
107. Nelson P, Baldwin D, Scearce L, Oberholtzer J, Tobias J, Mourelatos Z. Microarray-based, high-throughput gene expression profiling of microRNAs. *Nat Methods*. 2004;1(2):155–161. doi:10.1038/nmeth717
108. Sun X, Wang H, Jian Y, et al. Ultrasensitive microfluidic paper-based electrochemical/visual biosensor based on spherical-like cerium dioxide catalyst for miR-21 detection. *Biosens Bioelectron*. 2018;105:218–225. doi:10.1016/j.bios.2018.01.025
109. Zhang P, Wu X, Yuan R, Chai Y. An “off-on” electrochemiluminescent biosensor based on DNAzyme-assisted target recycling and rolling circle amplifications for ultrasensitive detection of microRNA. *Anal Chem*. 2015;87(6):3202–3207. doi:10.1021/ac504455z
110. Kichmazova NV, Bukharova EN, Selivanov NY, Bukharova IA, Karpunina LV. Preparation, properties and potential applications of exopolysaccharides from bacteria of the genera xanthobacter and ancylobater. *Appl Biochem Micro+*. 2017;53(3):325–330. doi:10.1134/S0003683817030073
111. Li J, Li D, Yuan R, Xiang Y. Biodegradable MnO<sub>2</sub> nanosheet-mediated signal amplification in living cells enables sensitive detection of down-regulated intracellular MicroRNA. *ACS Appl Mater Interfaces*. 2017;9(7):5717–5724. doi:10.1021/acsami.6b13073
112. Yang K, Zeng M, Hu X, Guo B, Zhou J. Layered MnO<sub>2</sub> nanosheet as a label-free nanoplateform for rapid detection of mercury(II). *Analyst*. 2014;139(18):4445–4448. doi:10.1039/c4an00649f
113. Yuan Y, Wu S, Shu F, Liu Z. An MnO<sub>2</sub> nanosheet as a label-free nanoplateform for homogeneous biosensing. *Chem Commun (Camb)*. 2014;50(9):1095–1097. doi:10.1039/c3cc47755j
114. Zhai W, Wang C, Yu P, Wang Y, Mao L. Single-layer MnO<sub>2</sub> nanosheets suppressed fluorescence of 7-hydroxycoumarin: mechanistic study and application for sensitive sensing of ascorbic acid in vivo. *Anal Chem*. 2014;86(24):12206–12213. doi:10.1021/ac503215z

115. Qi L, Yan Z, Huo Y, Hai X, Zhang Z. MnO nanosheet-assisted ligand-DNA interaction-based fluorescence polarization biosensor for the detection of Ag ions. *Biosens Bioelectron.* 2017;87:566–571. doi:10.1016/j.bios.2016.08.093
116. Tan Q, Zhang R, Kong R, Kong W, Zhao W, Qu F. Detection of glutathione based on MnO nanosheet-gated mesoporous silica nanoparticles and target induced release of glucose measured with a portable glucose meter. *Mikrochim Acta.* 2017;185(1):44. doi:10.1007/s00604-017-2586-4
117. Jalani G, Tam V, Vetrone F, Cerruti M. Seeing, targeting and delivering with upconverting nanoparticles. *J Am Chem Soc.* 2018;140:10923–10931. doi:10.1021/jacs.8b03977
118. Yang Z, Cheng R, Zhao C, et al. Thermo- and pH-dual responsive polymeric micelles with upper critical solution temperature behavior for photoacoustic imaging-guided synergistic chemo-photothermal therapy against subcutaneous and metastatic breast tumors. *Theranostics.* 2018;8(15):4097–4115. doi:10.7150/thno.26195
119. Langton M, Keymeulen F, Ciaccia M, Williams N, Hunter C. Controlled membrane translocation provides a mechanism for signal transduction and amplification. *Nat Chem.* 2017;9(5):426–430. doi:10.1038/nchem.2678
120. Niu D, Li Y, Shi J. Silica/organosilica cross-linked block copolymer micelles: a versatile theranostic platform. *Chem Soc Rev.* 2017;46(3):569–585. doi:10.1039/c6cs00495d
121. Yao C, Wang P, Li X, et al. Near-infrared-triggered azobenzene-liposome/upconversion nanoparticle hybrid vesicles for remotely controlled drug delivery to overcome cancer multi-drug resistance. *Adv Mater Weinheim.* 2016;28(42):9341–9348. doi:10.1002/adma.201503799
122. Datz S, Illes B, Gößl D, Schirnding C, Engelke H, Bein T. Biocompatible crosslinked  $\beta$ -cyclodextrin nanoparticles as multifunctional carriers for cellular delivery. *Nanoscale.* 2018;10:16284–16292. doi:10.1039/c8nr02462f
123. Zhang D, Yang J, Guan J, et al. In vivo tailor-made protein corona of a prodrug-based nanoassembly fabricated by redox dual-sensitive paclitaxel prodrug for the superselective treatment of breast cancer. *Biomater Sci.* 2018;6(9):2360–2374. doi:10.1039/c8bm00548f
124. Behroozi F, Abdkhodaie M, Abandansari H, et al. Engineering folate-targeting diselenide-containing triblock copolymer as a redox-responsive shell-sheddable micelle for antitumor therapy in vivo. *Acta Biomater.* 2018;76:239–256. doi:10.1016/j.actbio.2018.05.031
125. Yu J, Zhang Y, Kahkoska A, Gu Z. Bioresponsive transcutaneous patches. *Curr Opin Biotechnol.* 2017;48:28–32. doi:10.1016/j.copbio.2017.03.001
126. Hu J, Chen Y, Li Y, Zhou Z, Cheng Y. A thermo-degradable hydrogel with light-tunable degradation and drug release. *Biomaterials.* 2017;112:133–140. doi:10.1016/j.biomaterials.2016.10.015
127. Ji H, Dong K, Yan Z, et al. Bacterial hyaluronidase self-triggered prodrug release for chemo-photothermal synergistic treatment of bacterial infection. *Small.* 2016;12(45):6200–6206. doi:10.1002/smll.201601729
128. Timko B, Dvir T, Kohane D. Remotely triggerable drug delivery systems. *Adv Mater Weinheim.* 2010;22(44):4925–4943. doi:10.1002/adma.201002072
129. Agrawal G, Agrawal R. Functional microgels: recent advances in their biomedical applications. *Small.* 2018;14:e1801724. doi:10.1002/smll.v14.39
130. He Q, Kiesewetter D, Qu Y, et al. NIR-responsive on-demand release of CO from metal carbonyl-caged graphene oxide nanomedicine. *Adv Mater Weinheim.* 2015;27(42):6741–6746. doi:10.1002/adma.201502762
131. Lukianova-Hleb E, Ren X, Sawant R, Wu X, Torchilin V, Lapotko D. On-demand intracellular amplification of chemoradiation with cancer-specific plasmonic nanobubbles. *Nat Med.* 2014;20(7):778–784. doi:10.1038/nm.3484
132. Wang C, Seo S, Kim J, et al. Intravitreal implantable magnetic micropump for on-demand VEGFR-targeted drug delivery. *J Control Release.* 2018;283:105–112. doi:10.1016/j.jconrel.2018.05.030
133. Andreeva D, Cherepanov P, Avadhut Y, Senker J. Rapidly oscillating microbubbles force development of micro- and mesoporous interfaces and composition gradients in solids. *Ultrason Sonochem.* 2018;51:439–443. doi:10.1016/j.ultsonch.2018.07.024
134. Nguyen V, Ahmed A, Ramanujan R. Morphing soft magnetic composites. *Adv Mater Weinheim.* 2012;24(30):4041–4054. doi:10.1002/adma.201104994
135. Zhang D, Wei L, Zhong M, Xiao L, Li H, Wang J. The morphology and surface charge-dependent cellular uptake efficiency of upconversion nanostructures revealed by single-particle optical microscopy. *Chem Sci.* 2018;9(23):5260–5269. doi:10.1039/c8sc01828f
136. Lai W, Rogach A, Wong W. Molecular design of upconversion nanoparticles for gene delivery. *Chem Sci.* 2017;8(11):7339–7358. doi:10.1039/c7sc02956j
137. Wolfbeis O. An overview of nanoparticles commonly used in fluorescent bioimaging. *Chem Soc Rev.* 2015;44(14):4743–4768. doi:10.1039/c4cs00392f
138. Zhao P, Zhu Y, Yang X, et al. Multifunctional MnO<sub>2</sub> nanosheet-modified Fe<sub>3</sub>O<sub>4</sub>@SiO<sub>2</sub>/NaYF<sub>4</sub>: yb,Er nanocomposites as novel drug carriers. *Dalton Trans.* 2014;43(2):451–457. doi:10.1039/c3dt52066h
139. Pykett IL, Newhouse JH, Buonanno FS, et al. Principles of nuclear magnetic resonance imaging. *Radiology.* 1982;143(1):157–168. doi:10.1148/radiology.143.1.7038763
140. Nitz WR. [Magnetic resonance imaging. Sequence acronyms and other abbreviations in MR imaging]. *Radiologe.* 2003;43(9):745–763.
141. Armstrong P, Keevil SF. Magnetic resonance imaging—1: basic principles of image production. *BMJ (Clinical Research Ed).* 1991;303(6793):35–40. doi:10.1136/bmj.303.6793.35
142. Terreno E, Castelli D, Viale A, Aime S. Challenges for molecular magnetic resonance imaging. *Chem Rev.* 2010;110(5):3019–3042. doi:10.1021/cr100025t
143. Zhang S, Merritt M, Woessner D, Lenkinski R, Sherry A. PARACEST agents: modulating MRI contrast via water proton exchange. *Acc Chem Res.* 2003;36(10):783–790. doi:10.1021/ar020228m
144. Duboc C. Determination and prediction of the magnetic anisotropy of Mn ions. *Chem Soc Rev.* 2016;45(21):5834–5847. doi:10.1039/c5cs00898k
145. Weinmann H, Brasch R, Press W, Wesbey G. Characteristics of gadolinium-DTPA complex: a potential NMR contrast agent. *AJR Am J Roentgenol.* 1984;142(3):619–624. doi:10.2214/ajr.142.3.619
146. Schmidt-Lauber C, Bossaller L, Abujudeh H, et al. Gadolinium-based compounds induce NLRP3-dependent IL-1 $\beta$  production and peritoneal inflammation. *Ann Rheum Dis.* 2015;74(11):2062–2069. doi:10.1136/annrheumdis-2013-204900
147. Ilatovskaya D, Palygin O, Chubinskiy-Nadezhdin V, et al. Angiotensin II has acute effects on TRPC6 channels in podocytes of freshly isolated glomeruli. *Kidney Int.* 2014;86(3):506–514. doi:10.1038/ki.2014.71
148. Schieren G, Wirtz N, Altmeyer P, Rump L, Weiner S, Kreuter A. Nephrogenic systemic fibrosis—a rapidly progressive disabling disease with limited therapeutic options. *J Am Acad Dermatol.* 2009;61(5):868–874. doi:10.1016/j.jaad.2009.03.040
149. Runge V. Dechelation (Transmetalation): consequences and safety concerns with the linear gadolinium-based contrast agents, in view of recent health care rulings by the EMA (Europe), FDA (United States), and PMDA (Japan). *Invest Radiol.* 2018;53:571–578. doi:10.1097/RLI.0000000000000507

150. Zhao Z, Fan H, Zhou G, et al. Activatable fluorescence/MRI bimodal platform for tumor cell imaging via MnO<sub>2</sub> nanosheet-aptamer nanoprobe. *J Am Chem Soc.* 2014;136(32):11220–11223. doi:10.1021/ja5029364
151. Zhang X, Zheng C, Guo S, Li J, Yang H, Chen G. Turn-on fluorescence sensor for intracellular imaging of glutathione using g-C<sub>3</sub>N<sub>4</sub> nanosheet-MnO<sub>2</sub> sandwich nanocomposite. *Anal Chem.* 2014;86(7):3426–3434. doi:10.1021/ac500336f
152. Fan D, Shang C, Gu W, Wang E, Dong S. Introducing ratiometric fluorescence to MnO nanosheet-based biosensing: a simple, label-free ratiometric fluorescent sensor programmed by cascade logic circuit for ultrasensitive GSH detection. *ACS Appl Mater Interfaces.* 2017;9(31):25870–25877. doi:10.1021/acsami.7b07369
153. Marcel Y, Jewer D, Leblond L, Weech P, Milne R. Lipid peroxidation changes the expression of specific epitopes of apolipoprotein A-I. *J Biol Chem.* 1989;264(33):19942–19950.
154. Wang D, Lin H, Zhang G, et al. An effectively pH-activated theranostic platform for synchronous magnetic resonance imaging diagnosis and chemotherapy. *ACS Appl Mater Interfaces.* 2018;10:31114–31123. doi:10.1021/acsami.8b11408
155. Yang Y, Zhu W, Dong Z, et al. 1D coordination polymer nanofibers for low-temperature photothermal therapy. *Adv Mater Weinheim.* 2017;29(40):1703588. doi:10.1002/adma.201700681
156. Chen Y, Ye D, Wu M, et al. Break-up of two-dimensional MnO<sub>2</sub> nanosheets promotes ultrasensitive pH-triggered theranostics of cancer. *Adv Mater Weinheim.* 2014;26(41):7019–7026. doi:10.1002/adma.201402572
157. Shi W, Song B, Shi W, et al. A bimodal phosphorescence-magnetic resonance imaging nanoprobe for glutathione based on MnO<sub>2</sub> nanosheet-Ru(II) complex nanoarchitecture. *ACS Appl Mater Interfaces.* 2018;10:27681–27691. doi:10.1021/acsami.8b08872
158. Peng CH, Cherng JY, Chiou GY, et al. Delivery of Oct4 and SirT1 with cationic polyurethanes-short branch PEI to aged retinal pigment epithelium. *Biomaterials.* 2011;32(34):9077–9088. doi:10.1016/j.biomaterials.2011.08.008
159. Tang Z, Liu Y, He M, Bu W. Chemodynamic therapy: tumour microenvironment-mediated fenton and fenton-like reaction. *Angew Chem Int Ed Engl.* 2018;58:946–956. doi:10.1002/anie.201805664
160. Liu Y, Jia Q, Guo Q, Wei W, Zhou J. Simultaneously activating highly selective ratiometric MRI and synergistic therapy in response to intratumoral oxidability and acidity. *Biomaterials.* 2018;180:104–116. doi:10.1016/j.biomaterials.2018.07.025
161. Lin H, Chen Y, Shi J. Nanoparticle-triggered in situ catalytic chemical reactions for tumour-specific therapy. *Chem Soc Rev.* 2018;47(6):1938–1958. doi:10.1039/c7cs00471k
162. Tang Z, Zhang H, Liu Y, et al. Antiferromagnetic pyrite as the tumor microenvironment-mediated nanopatform for self-enhanced tumor imaging and therapy. *Adv Mater Weinheim.* 2017;29(47):1701683. doi:10.1002/adma.201700681
163. Stockwell B, Friedmann Angeli J, Bayir H, et al. Ferroptosis: a regulated cell death nexus linking metabolism, redox biology, and disease. *Cell.* 2017;171(2):273–285. doi:10.1016/j.cell.2017.09.021
164. Shen Z, Song J, Yung B, Zhou Z, Wu A, Chen X. Emerging strategies of cancer therapy based on ferroptosis. *Adv Mater Weinheim.* 2018;30(12):e1704007. doi:10.1002/adma.201704007
165. Vanden Berghe T, Linkermann A, Jouan-Lanhouet S, Walczak H, Vandenabeele P. Regulated necrosis: the expanding network of non-apoptotic cell death pathways. *Nat Rev Mol Cell Biol.* 2014;15(2):135–147. doi:10.1038/nrm3737
166. Conrad M, Angeli J, Vandenabeele P, Stockwell B. Regulated necrosis: disease relevance and therapeutic opportunities. *Nat Rev Drug Discov.* 2016;15(5):348–366. doi:10.1038/nrd.2015.6
167. Kim S, Zhang L, Ma K, et al. Ultrasmall nanoparticles induce ferroptosis in nutrient-deprived cancer cells and suppress tumour growth. *Nat Nanotechnol.* 2016;11(11):977–985. doi:10.1038/nnano.2016.164
168. Liu Y, Zhen W, Jin L, et al. All-in-one theranostic nanoagent with enhanced reactive oxygen species generation and modulating tumor microenvironment ability for effective tumor eradication. *ACS Nano.* 2018;12(5):4886–4893. doi:10.1021/acs.nano.8b01893
169. Fan J, Ye J, Kamphorst J, Shlomi T, Thompson C, Rabinowitz J. Quantitative flux analysis reveals folate-dependent NADPH production. *Nature.* 2014;510(7504):298–302. doi:10.1038/nature13236
170. He D, Yang X, He X, et al. A sensitive turn-on fluorescent probe for intracellular imaging of glutathione using single-layer MnO<sub>2</sub> nanosheet-quenched fluorescent carbon quantum dots. *Chem Commun (Camb).* 2015;51(79):14764–14767. doi:10.1039/c5cc05416h
171. Ou M, Huang J, Yang X, et al. Live-cell microRNA imaging through MnO nanosheet-mediated DD-A hybridization chain reaction. *Chembiochem.* 2018;19(2):147–152. doi:10.1002/cbic.201700573
172. Ou M, Huang J, Yang X, et al. MnO nanosheet mediated “DD-A” FRET binary probes for sensitive detection of intracellular mRNA. *Chem Sci.* 2017;8(1):668–673. doi:10.1039/c6sc03162e